


RESEARCH ARTICLE

How well does the local climate zone scheme discern the thermal environment of Toulouse (France)? An analysis using numerical simulation data

Yu Ting Kwok¹  | Robert Schoetter² | Kevin Ka-Lun Lau³ | Julia Hidalgo⁴ |
Chao Ren^{1,3} | Grégoire Pigeon² | Valéry Masson²

¹School of Architecture, The Chinese University of Hong Kong, Hong Kong, China

²CNRM, Université de Toulouse, Météo-France, CNRS, Toulouse Cedex 1, France

³Institute of Future Cities, The Chinese University of Hong Kong, Hong Kong, China

⁴LISST UMR 5193, CNRS/UT2J, Toulouse Cedex 1, France

Correspondence

Yu Ting Kwok, School of Architecture, The Chinese University of Hong Kong, Shatin, New Territories, Hong Kong, China.
Email: ytkwok@link.cuhk.edu.hk

Present address

Chao Ren, Faculty of Architecture, The University of Hong Kong, Pokfulam, Hong Kong, China.
Grégoire Pigeon, MetService, 30 Salamanca Road, Kelburn, Wellington 6012 PO Box 722, Wellington 6140, New Zealand.

Funding information

Agence Nationale de la Recherche, Grant/Award Number: ANR-13-VBDU-0004; Chinese University of Hong Kong, Grant/Award Number: The Vice-Chancellor's Discretionary Fund

Abstract

To build healthy, resilient, and climate-responsive cities, planners need ways to understand the local complexities of urban thermal climates. To assist in meeting this need, this study employs the simple classification of “local climate zones” (LCZs) to conduct a spatiotemporal thermal climatic analysis of the Toulouse Metropolitan Region (France) under warm and dry summer conditions. Simulations are performed using the mesoscale atmospheric model MésO-NH. These simulations provide a city-wide spatial coverage of 2-m air temperature (T2M), mean radiant temperature (MRT), and Universal Thermal Climate Index (UTCI). Model parameters describing the urban morphology are initialized based on administrative databases and independent of LCZ maps, which allows for an evaluation of whether the distributions of the modelled thermal climatic parameters will differ between LCZs. The results show that different LCZs possess significantly different distributions of T2M and MRT, confirming the suitability of the LCZ scheme for discerning the thermal environment of Toulouse. Compact urban settings (LCZ 1/2/3) show the highest T2M throughout the day and a nocturnal temperature difference of up to 2.8 K compared to rural settings. The MRT of LCZ 1/2/3 in the late afternoon (1700–2000 LST (UTC + 2)) can be as much as 6.3 K lower than it is for LCZs with open settings due to shading by dense urban structures. Additional analysis reveals that the intra-LCZ variabilities of T2M and MRT may be explained by the distance to the city centre. Finally, the thermal stress in different LCZs is assessed with the modelled UTCI. Among the built LCZs, the probability of strong heat stress is the highest for open high/mid-rise (LCZ 4/5) and lowest for sparsely built (LCZ 9) and open low-rise (LCZ 6) settings. For land cover type LCZs, dense trees (LCZ A) are the most favourable for daytime outdoor human thermal comfort.

KEYWORDS

heat stress, local climate zones, numerical model simulation, universal thermal climate index (UTCI), urban climate analysis, urban thermal environment

1 | INTRODUCTION

Urban climate research has pointed unanimously to the fact that urban built environments, alongside the human activities within, alter the surface energy balance in urban areas and thus create the thermal environments characteristic of cities (Oke *et al.*, 2017). One of the most well-documented climate phenomena resulting from urbanization is the urban heat island (UHI), which refers to the general observation of higher air temperatures in urban areas compared to their rural surroundings (Arnfield, 2003). However, the differentiation between “urban” and “rural” in conventional UHI studies worldwide has been rather vague and over-simplified such that the spatial heterogeneity of near-surface air temperatures induced by their underlying land covers could not be accurately described (Stewart, 2011). The “local climate zone” (LCZ) concept has therefore been introduced by Stewart and Oke (2012) to more objectively classify “urban” and “rural” land covers based on their influence on the local air temperature.

The primary objective of the LCZ scheme is to enable a standardized selection of urban measurement sites and the documentation of UHI intensities (Stewart and Oke, 2012). Developed to expand and improve previous works on the “urban climate zone” (UCZ) classification (Oke, 2004), the LCZ scheme comprises ten “built” and seven “land cover” classes, which are defined as regions spanning hundreds of meters to a few kilometres with similar physical surface properties that influence the local climate, such as the sky view factor (SVF), building surface fraction, impervious surface fraction, terrain roughness, surface albedo, and anthropogenic heat flux. The inter-LCZ temperature difference ($\Delta T_{LCZ\ x-y}$) can then be conveniently used to quantify the UHI intensity (Stewart *et al.*, 2014).

An important research topic is the development of methodologies to produce LCZ maps for any given urban agglomeration in the world. Ideally, the mapping of urban and rural areas into LCZs should be based on detailed urban morphological data, but they are not always available. New techniques have therefore been developed based on remote sensing technologies to obtain LCZ data for cities in which such information is otherwise inaccessible (Lelovics *et al.*, 2014; Bechtel *et al.*, 2015; Geletič and Lehnert, 2016) and to automate LCZ mapping procedures. In France, where detailed urban data are available for the entire country, a newly proposed bottom-up, semi-automatic method that accounts for regional variations in morphological indicators to generate more precise LCZ maps within a geographic information system (GIS) has been tested (Hidalgo *et al.*, 2019). The LCZ map for Toulouse will be used to evaluate inter- and intra-LCZ temperature differences in this study.

Numerous studies have been conducted to support the LCZ classification with climatological data and to evaluate temperature differences among LCZs. Following the first assessment of the LCZ scheme by Stewart *et al.* (2014) using screen-height temperatures observed in Nagano (Japan), Vancouver (Canada), and Uppsala (Sweden), studies have been performed in multiple European cities, such as Dublin (Alexander and Mills, 2014), Olomouc (Lehnert *et al.*, 2015), Szeged (Skarbit *et al.*, 2017), Berlin (Fenner *et al.*, 2017), and Augsburg (Beck *et al.*, 2018) to reveal distinct air temperature signals for stations located in different LCZs. However, one major drawback of using station “point” measurements is the inability to capture spatial variations in temperature in detail. Mobile measurements of air temperatures have been performed in Nancy (Leconte *et al.*, 2015), but the data coverage is still limited by the spatial extent of the survey routes.

As urban land surface models increase in model complexity and resolution (Grimmond *et al.*, 2010), modelled data from numerical simulations offer another option for evaluating the intra-urban temperature distribution across the entire city with extensive spatial coverage and a better sampling for each LCZ (Stewart *et al.*, 2014; Verdonck *et al.*, 2017; 2018); however, this method has been less frequently explored to date. This might be because model results are subject to uncertainties, for example, due to the employed numerical methods and the simplified representation of physical processes. The realism of numerical model results therefore needs to be carefully evaluated. Furthermore, model parameters describing the urban morphology need to be initialized independent of the LCZs in order to allow for a correct attribution of differences in the modelled thermal climatic parameters relative to the differences between LCZs. Nonetheless, numerical models present some advantages over observational data since they preserve the physical consistency between meteorological parameters and enable the simulation of scenarios (e.g., urban development, heat stress mitigation strategies, and future climate conditions).

Besides varying spatially, the thermal characteristics of LCZs and UHI intensities also vary with different times of the year and day. Seasonal variability can be observed in Nagano, where the temperature difference between LCZ 3 (compact low-rise) and LCZ D (low plants) shows a remarkable decrease in spring/summer due to the changes in land surface properties caused by the flooding of rice fields (Stewart *et al.*, 2014). Houet and Pigeon (2011) and Fenner *et al.* (2017) have also reported annual variabilities in the inter-UCZ/LCZ temperature differences, and observation-based studies generally indicate that cloud-free days with low wind speeds in the summer favour pronounced temperature differences between LCZs (e.g., Alexander and Mills,

2014; Lehnert *et al.*, 2015; Fenner *et al.*, 2017). Regarding the diurnal variability, the UHI is commonly known as a nocturnal phenomenon (Oke, 1981; Cleugh and Grimmond, 2012), which has been confirmed by previous UHI studies using the LCZ concept (Alexander and Mills, 2014; Leconte *et al.*, 2015; Fenner *et al.*, 2017; Skarbit *et al.*, 2017). During the day, however, the temperature contrast between “urban” and “rural” LCZs becomes less evident, and it may even be reversed owing to shading within compact urban structures (Erell and Williamson, 2007; Hidalgo *et al.*, 2008; Houet and Pigeon, 2011; Middel *et al.*, 2014); this phenomenon is denoted as an “urban cool island.”

There have been many studies regarding the impacts of heat in urban areas on human health and mortality (e.g., Buechley *et al.*, 1972; Gosling *et al.*, 2009; Tan *et al.*, 2010; Gabriel and Endlicher, 2011). Prolonged exposure to high air temperatures, especially at night, weakens the human body by preventing its recovery from daytime heat gain (Laaidi *et al.*, 2012). Its effect has been reflected in the excess deaths recorded in European cities during the 2003 heatwave (Conti *et al.*, 2005; Grize *et al.*, 2005; Fouillet *et al.*, 2006). Results illustrating different local thermal climates with respect to LCZs may therefore help to inform decisions about the heat-related health risks in various parts of the city using observed and modelled air temperatures as indicators (e.g., Verdonck *et al.*, 2018). Another relevant indicator of human thermal perception in outdoor environments is the radiant temperature (Lin, 2009). However, since the LCZ scheme was designed for air temperatures, only few studies investigated the relationship between LCZs and the radiant temperature (Sharmin *et al.*, 2015; Aminipouri *et al.*, 2019). They found potential reduction in radiant temperature and improvement in thermal comfort by varying building form and planting street trees. This relationship will be further addressed in the current study.

Apart from studies on the air temperature differences between LCZs, attempts have been made to evaluate outdoor thermal comfort conditions for different LCZs using physiological equivalent temperatures (PET) calculated from station measurements (Kovács and Németh, 2012; Van Hove *et al.*, 2015; Milošević *et al.*, 2016; Unger *et al.*, 2018) and thermal sensation votes obtained from field surveys (Villadiego and Velay-Dabat, 2014). Other studies (Müller *et al.*, 2014; Geletič *et al.*, 2018) have examined the spatio-temporal variability of outdoor human thermal comfort with respect to LCZs and relevant adaptation scenarios to reduce heat stress with the help of numerical model simulations. Understanding both the temporal and spatial distribution of thermal comfort indicators in cities could provide urban planners with helpful information for climate-responsive planning and the formulation of city-wide heat stress

mitigation strategies (Koppe *et al.*, 2004; Kleerekoper *et al.*, 2012).

This study falls within the framework of the French national MApUCE (applied Modeling and urbAn Planning laws: Urban Climate and Energy) project, which aims to integrate quantitative data on the urban microclimate, climate, and energy into urban policies and relevant French legal documents (Masson *et al.*, 2015). The overarching research question of this article is to determine how well the LCZ scheme discerns the thermal environment of Toulouse. The specific research steps for achieving this objective are as follows:

1. To obtain the thermal climatic parameters, namely the 2-m air temperature (T2M), the mean radiant temperature (MRT), and the Universal Thermal Climate Index (UTCI), for the Toulouse Metropolitan Region under typical summer conditions by performing hindcast simulations using the mesoscale atmospheric model Méso-NH and evaluating the model outputs against observations.
2. To examine the spatiotemporal variations in the urban thermal environment and heat stress during typical summer conditions in the Toulouse Metropolitan Region by analysing inter- and intra-LCZ differences in T2M, MRT, and UTCI, for three time periods during the day.
3. To investigate whether LCZs possess distinct thermal characteristics based on numerical simulation data. Since the data describing the urban morphology in the model has been derived from administrative data sets independently of the LCZ delimitation, the results can be used to evaluate the suitability of the LCZ scheme to discriminate among the thermal climatic conditions in Toulouse.

2 | METHODOLOGY

2.1 | Study area

In France, an urban unit corresponds to “a municipality or a group of municipalities that includes a continuously built-up zone and at least 2,000 inhabitants” (Institut national de la statistique et des études économiques (Insee), 2016). The urban unit of Toulouse (centred at 43.60°N, 1.44°E; Figure 1a) has been selected for an exemplary case study within the MApUCE project. It is situated in the southwestern part of France, 80 km north of the Pyrénées mountain chain, 150 km west of the Mediterranean Coast, and 250 km east of the Atlantic Ocean. Toulouse experiences a “degraded oceanic climate” and does not benefit from the cooling brought by valley or coastal breezes. Its geographical location gives rise to its four marked seasons: mild wet springs, dry and hot summers, sunny and mild autumns, and relatively cold and wet winters. Although Toulouse is the fourth-largest agglomeration in France with over 1.3 million

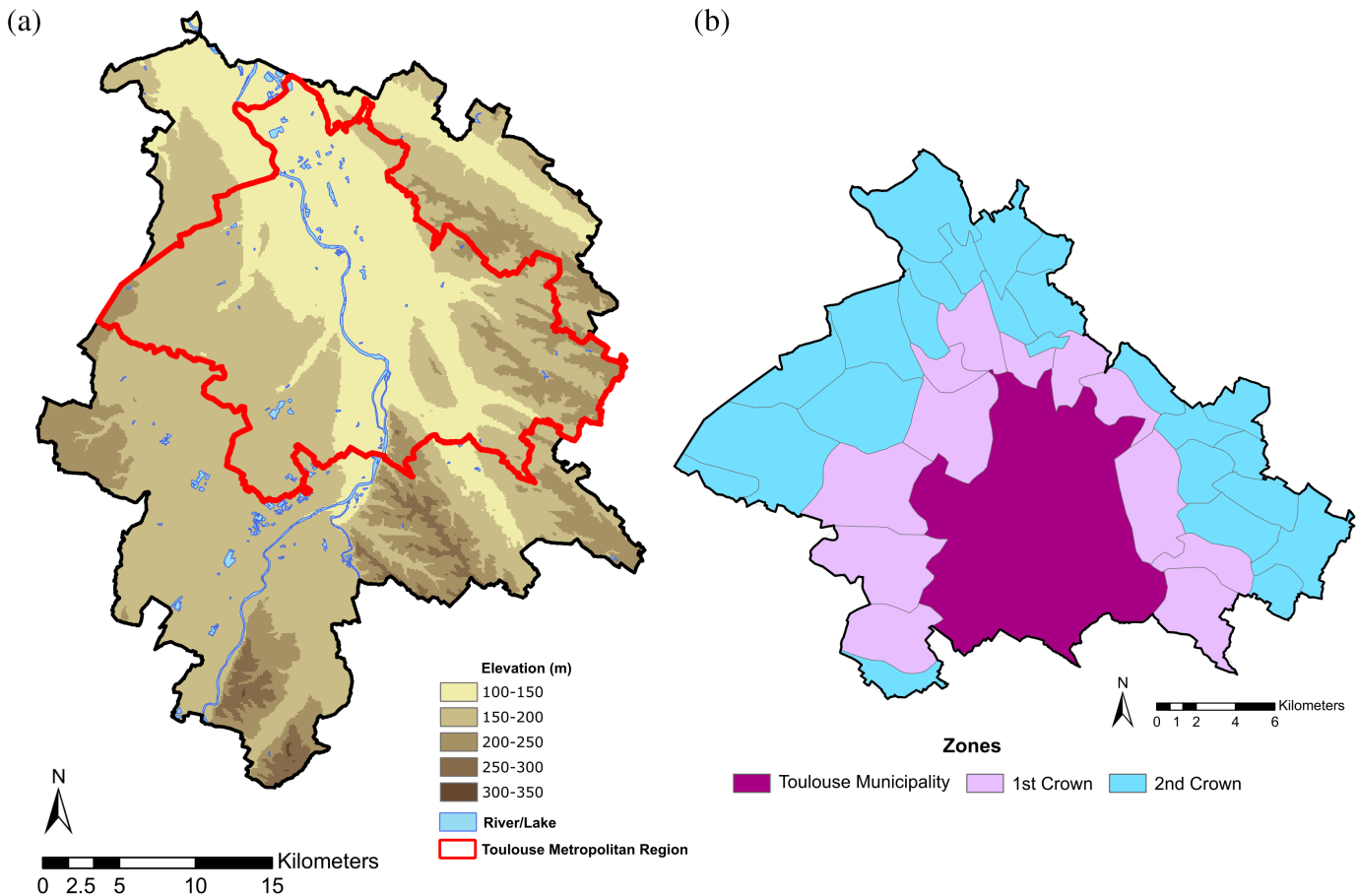


FIGURE 1 (a) Topography of the urban unit of Toulouse, the thick red line shows the administrative boundary of the Toulouse Metropolitan Region; (b) communes within the Toulouse Metropolitan Region and the three regions defined for the thermal climatic analysis [Colour figure can be viewed at wileyonlinelibrary.com]

inhabitants, its large area of 1,175 km² makes it one of the least dense cities in France.

A thermal climatic analysis is performed for the area within the administrative boundary of the Toulouse Metropolitan Region (Figure 1a). The Toulouse Metropolitan Region has a relatively flat relief with elevations between 100 and 300 m. It lies within the affluent valleys of the river Garonne, the primary channel of which runs through the city centre. The Toulouse Metropolitan Region is further separated into 37 communes, each having their own town centres. These communes are split into Toulouse Municipality, first Crown (communes in the immediate periphery of Toulouse Municipality), and second Crown (the remaining communes) (Figure 1b) to facilitate a further investigation of the inter- and intra-LCZs differences in the thermal climatic parameters.

2.2 | Local climate zone map of Toulouse

The LCZ map of Toulouse (Figure 2) was generated at the building block scale in a GIS platform using a semi-

automatic statistical method (Hidalgo *et al.*, 2019) as applied to urban morphology parameters acquired from administrative and topographic databases as part of the MApUCE project (Bocher *et al.*, 2018). Built LCZs were categorized according to seven indicators, including the building surface fraction, building height, minimum distance between buildings, and building typologies as defined by Tornay *et al.* (2017). Next, water (LCZ G) and bare rock/paved (LCZ E) were classified. Information on the vegetation cover was retrieved from satellite images (Crombette *et al.*, 2014); this approach allowed for the determination of dense trees (LCZ A), scattered trees (LCZ B), and low plants (LCZ D). Finally, the remaining non-classified areas were attributed to LCZ D. Due to the limitations of the MApUCE database, heavy industry (LCZ 10), bush/scrub (LCZ C), and bare soil (LCZ F) could not be properly defined.

The most common built LCZ in Toulouse is open low-rise (LCZ 6), reflecting the city's low built density (Figure 2). The second-most common LCZ is large low-rise (LCZ 8). It corresponds to commercial and industrial

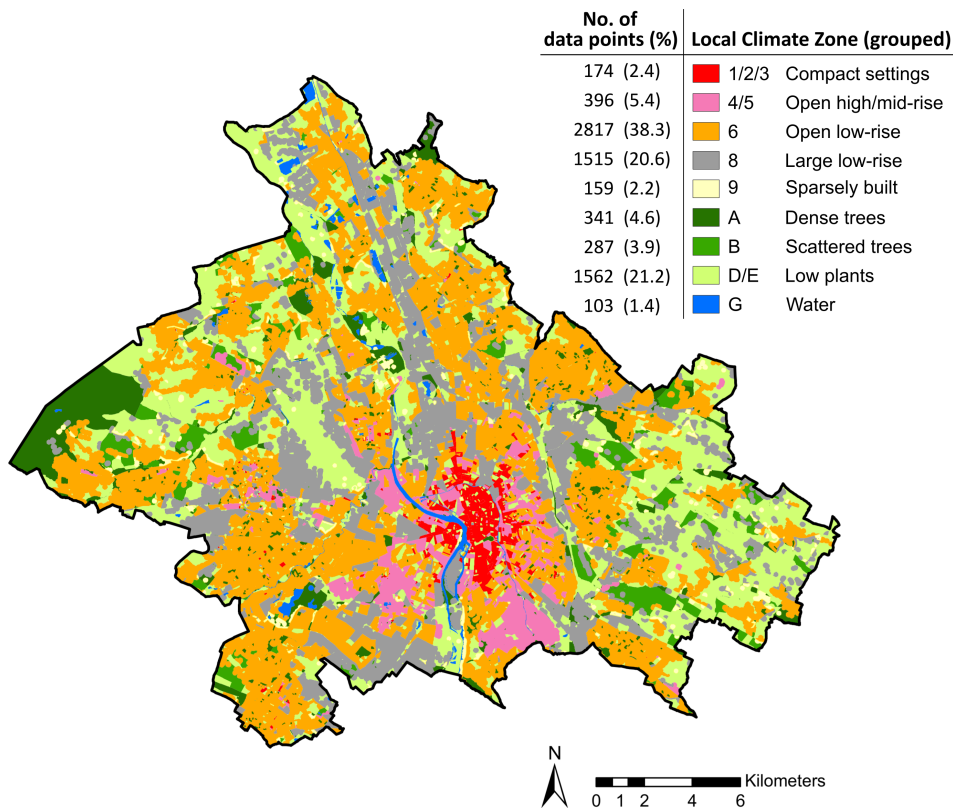


FIGURE 2 Grouped LCZ map of the Toulouse Metropolitan Region with the number and percentage of data points for each LCZ group [Colour figure can be viewed at wileyonlinelibrary.com]

developments that concentrate along major traffic routes radiating from the city centre. Within the Toulouse Municipality, the historical town centre consists mainly of compact mid-rise (LCZ 2) buildings with patches of open mid-rise (LCZ 5) and compact low-rise (LCZ 3) buildings in its immediate periphery. There are few informal settlements in Toulouse, and thus lightweight low-rise (LCZ 7) buildings are not present at the building block scale. For natural land covers, the predominant type is LCZ D, which occurs as non-irrigated farmlands with “Atlantic coast crops” in the western part and “warm temperate crops” in the eastern part (ECOCLIMAP-I land cover types; Champeaux *et al.*, 2005) of the first and second Crowns. LCZ A and LCZ B are present in scattered patches, except for the Bouconne Forest (LCZ A) in the west.

2.3 | Selection of meteorological situations and thermal climatic parameters

Hidalgo *et al.* (2014) identified 11 typical meteorological situations (the so-called local weather types) for Toulouse, among which local weather type 9 (WT9) has the highest occurrence frequency in the weather records from 1998 to 2008, particularly in the summer. WT9 is characterized by warm and dry conditions, light northwesterly winds, and a large diurnal temperature range (Hidalgo and Jouglu, 2018). It favours the development of a strong nocturnal UHI and is

prone to heat stress. In this study, all 18 days showing WT9 conditions in June, July, and August (JJA) of 2004 are investigated. The year 2004 was selected because it coincides with the deployment of a dense station network within the framework of the CAPITOUUL campaign (Masson *et al.*, 2008), allowing for an evaluation of the model results against station measurements (section 3.2). To also account for the diurnal temperature variability on these selected days, hourly data for three time periods of interest are examined. The three time periods studied here are the early afternoon (EAFT; 1300–1600 LST) when the solar radiation is the strongest, late afternoon (LAFT; 1700–2000 LST) when the air temperature is the highest, and night-time (NIGHT; 0300–0600 LST of the night following a WT9 day) when the UHI effect is most prominent (Oke, 1981). The time periods were selected while noting that Toulouse experiences prolonged sunlit hours during the day (until sunset after 2100 LST) due to its relatively late solar noon (1400 LST) in the summer.

This study focuses on the following three model output parameters: the air temperature at 2 m above the ground (T2M), the mean radiant temperature (MRT), and the Universal Thermal Climate Index (UTCI). The air temperature is the most commonly used parameter in UHI studies. It is easy to measure and is also relevant for nocturnal thermal comfort since it affects the cooling potential of buildings via ventilation (window opening). MRT deals with the radiative

heat exchange between the human body and its surroundings (ASHRAE, 2013) and is an important component of the UTCI, which quantifies the thermal stress of a reference human body. The UTCI is designed to assess the actual impact of the thermal environment on a reference human body based on a heat balance model. The UTCI assessment scale defines thermal stress categories based on the physiological response of a human body to the prevailing environmental conditions (Table 1; Blazejczyk *et al.*, 2013). The UTCI thus allows for the thermal stress in each LCZ to be quantified.

2.4 | Urban thermal climatic analysis approach

To conduct the urban thermal climatic analysis, it is necessary to join the modelled thermal climatic parameters with the corresponding LCZs spatially. The model outputs (T2M, MRT, and UTCI) at a 250-m horizontal resolution are overlain onto the LCZ map in ArcGIS. Using the “Extract Values to Point” tool, each model output data point is matched with its underlying LCZ. For small isolated LCZs with an area below 10,000 m², the dominant LCZ within a 250 m buffer drawn around the data point is assigned to the point instead. This is done to better match the model resolution of 250 m, which cannot capture the sub-grid scale variation of meteorological parameters. After a preliminary analysis, some LCZs are grouped (i.e., LCZ 1/2/3, LCZ 4/5, LCZ D/E) based on their similar thermal properties and/or geographic proximity to avoid sample sizes that are too small for a fair statistical analysis of the differences between LCZs. The final LCZ map of the Toulouse Metropolitan Region used for this study and the corresponding number of data points for each LCZ group are shown in Figure 2.

The thermal climate analysis consists of four main parts. First, box plots are used to display the general statistical distribution of the meteorological variables (T2M and MRT) for different LCZs. Second, a one-way analysis of variance (ANOVA) is applied to test for the statistical significance of mean temperature differences among LCZs. A Kolmogorov–Smirnov test reveals that the statistical

distributions of both T2M and MRT deviate from a normal distribution. However, the robustness of the ANOVA is generally unaffected by non-normality for a sufficiently large sample size (Lix *et al.*, 1996; Blanca *et al.*, 2017), as is the case here. Since homogeneity of variance (as tested by a Levene's test) cannot be assumed, a Welch's ANOVA (Welch, 1951) is used instead of the classic one-way ANOVA. The nonparametric Games-Howell post hoc test (Games and Howell, 1976) is then employed to identify the pairs of LCZs for which their thermal climatic parameters are significantly different. In addition, the Holm-Bonferroni method (Holm, 1979) is adopted to adjust the *p*-values in the multiple hypothesis tests to minimize false positive results. A further analysis to examine the intra-LCZ variability of thermal characteristics is conducted by splitting the data set according to the three spatial regions (i.e., Toulouse Municipality, first Crown, and second Crown). Finally, the UTCI values are used to infer the probability that people may experience the different thermal stress categories listed in Table 1 for each LCZ. Because this inference is achieved by pooling all the UTCI values together for every hour during each selected 4-hr time period over the 18 WT9 days studied here (i.e., 72 values for each data point), both the spatial and temporal variations in the thermal stress probability can be considered.

3 | MESOSCALE ATMOSPHERIC MODEL SIMULATIONS

3.1 | Model configuration and technical details

The thermal climatic parameters must be simulated at a high spatial resolution in order to capture their spatial variability in the Toulouse Metropolitan Region. To this end, the non-hydrostatic mesoscale atmospheric model Méso-NH (Lac *et al.*, 2018) is employed. It is based on the fundamental physical conservation laws for momentum, mass and energy, as well as the ideal gas law. The equations are discretized on a staggered Arakawa-C grid and solved in flux form. The coordinate system follows the terrain.

Méso-NH is applied in hindcast mode and used to dynamically downscale the European Centre for Medium-Range Weather Forecasts (ECMWF) Integrated Forecasting System (IFS) high-resolution operational forecast analyses (Cycle 28r1 before 29 June 2004 and Cycle 28r2 thereafter with a horizontal resolution of approximately 40 km; European Centre for Medium-Range Weather Forecasts (ECMWF), 2019) via three intermediate nesting steps to a horizontal resolution of 250 m. The horizontal grid resolutions of the four domains are 8 km (D1), 2 km (D2), 1 km (D3), and 250 m (D4). D4 covers the entire Toulouse Metropolitan Region, and its horizontal resolution allows for the

TABLE 1 The UTCI assessment scale with UTCI ranges and their corresponding thermal stress categories according to Blazejczyk *et al.* (2013)

UTCI (°C) range	Thermal stress category
+38 to +46	Very strong heat stress
+32 to +38	Strong heat stress
+26 to +32	Moderate heat stress
+9 to +26	No thermal stress
0 to +9	Slight cold stress

TABLE 2 Overview of Méso-NH domain characteristics and employed physical parameterizations

Domain	Extent (km)	Horizontal resolution (km)	Time step (s)	Parameterization of deep convection	Parameterization of shallow convection and dry thermals	Mixing length calculation
D1	1,280 × 1,280	8	20	Kain and Fritsch (1990)	Pergaud <i>et al.</i> (2009)	Bougeault and Lacarrere (1989)
D2	320 × 320	2	20	None	Pergaud <i>et al.</i> (2009)	Bougeault and Lacarrere (1989)
D3	160 × 160	1	20	None	None	Bougeault and Lacarrere (1989)
D4	60 × 60	0.25	10	None	None	Deardorff (1980)

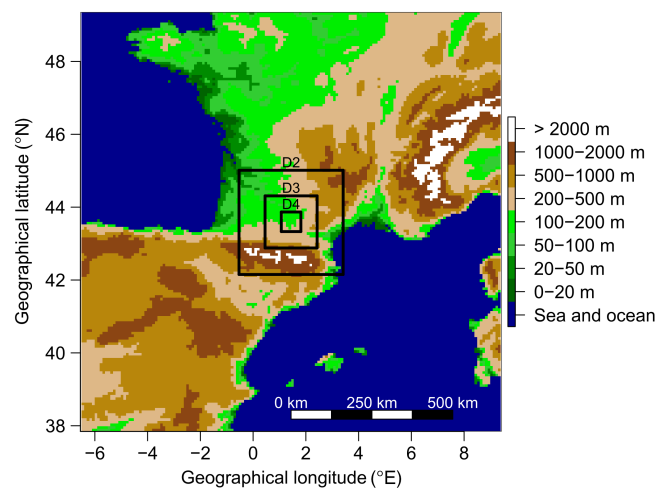
explicit representation of the largest turbulent eddies in the convective boundary layer. The domain sizes and physical parameterizations employed (Data S1, Supporting Information) are given in Table 2; the delimitation of the model domains is displayed in Figure 3. The initial conditions for all the domains and boundary conditions for D1 are taken from the ECMWF analysis data. The one-way grid nesting method is used for D2, D3, and D4.

There are 56 vertical levels. The first model level is 10 m above the ground. The vertical resolution is 20 m in the first 200 m of the atmosphere. Above that, the vertical resolution increases by 15% every grid point to a maximum of 1,000 m. There are 23 model levels below 1,000 m, and the model top is set at 18 km.

For each day *D* with WT9 conditions during JJA 2004, a Méso-NH simulation is initialized at $D - 2$, 0 UTC. Two entire days ($D - 2$ and $D - 1$) are simulated to allow for spin-up. The simulations end at $D + 1$, 24 UTC. The thermal climatic parameters for NIGHT are taken from the model results for day $D + 1$ since it is assumed that they are mostly shaped by the meteorological conditions experienced on day *D*.

The surface energy balance is not solved directly by Méso-NH. Instead, Méso-NH is coupled to the Externalised Surface (SURFEX; Masson *et al.*, 2013), which considers four different surface cover types as tiles within a single grid, namely TOWN (urban areas), NATURE (rural areas), SEA (seas and oceans), and WATER (lakes and rivers). It employs the urban canopy parameterization Town Energy Balance (TEB; Masson, 2000) for the TOWN tile and the Interactions between Soil, Biosphere, and Atmosphere (ISBA; Noilhan and Planton, 1989) for the NATURE tile. TEB assumes a simple 3D urban geometry with buildings aligned along street canyons and solves the surface energy budget separately for a representative roof, wall, and road. TEB is a single-layer urban canopy parameterization, which means that the exchanges with the atmospheric model occur

only at the first level of the atmospheric model. This assumption is reasonable for a city such as Toulouse in which high-rise buildings are rare. In addition to the basic version of TEB, the representation of in-canyon urban vegetation by Lemonsu *et al.* (2012) is used and the Building Energy Model (BEM; Bueno *et al.*, 2012) is employed to solve the energy budget of a representative building at the district scale. Furthermore, the surface boundary layer (SBL) scheme of Hamdi and Masson (2008) accounts for the drag effect due to buildings and the vertical distribution of sensible heat fluxes on walls and roofs to calculate vertical profiles of thermal climatic parameters in the street canyon. A similar SBL scheme is applied in rural areas (ISBA). An important restriction of the employed modelling approach is that in-canyon vegetation is treated as though it is located at the surface of the street canyon. This treatment affects the energy balance of the urban vegetation (e.g., too little solar radiation captured by street trees) and also human thermal

**FIGURE 3** Surface elevation of the outermost model domain (D1) and boundaries of the domains D2, D3, and D4 [Colour figure can be viewed at wileyonlinelibrary.com]

comfort since shading due to street trees is not considered. The employed modelling approach will therefore tend to overestimate the probability or severity of the heat stress. The explicit treatment of high vegetation implemented by Redon *et al.* (2017) will circumvent this restriction in future versions of TEB. Similarly, for rural areas, the ISBA vegetation model employed here also only considers the vegetation at the surface.

Data characterizing the urban structure and fabric (including the urban morphology, construction materials, and their physical properties) of Toulouse are taken from the MApUCE database (<http://mapuce.orbisgis.org/>). The TEB input parameters related to urban morphology, for example, the building surface fraction (Figure 4b), average building height (Figure 4c), and façade surface density (Figure 4d), have been calculated by Bocher *et al.* (2018) based on the building geometry data taken from the French digital basic

map BDTOPO as provided by the French National Geographical Institute. The parameters related to the construction materials (e.g., roof albedo, wall thermal conductivity) are initialized via the database on French building archetypes compiled by Tornay *et al.* (2017). The parameters related to building use and human behaviour relevant for BEM are initialized as described in Schoetter *et al.* (2017). Urban vegetation has been retrieved by processing satellite images (Crombette *et al.*, 2014). For the initialization of the land cover parameters of the rural areas surrounding Toulouse (e.g., forests, cropland), the 1-km resolution ECOCLIMAP-I database (Champeaux *et al.*, 2005) is adopted.

In the model, the thermal climatic parameters of interest are calculated separately for the four SURFEX tiles. Detailed equations and the assumptions made to calculate the thermal climatic parameters can be found in Data S2. The weighted average of T2M, obtained from the SBL level at 2 m above

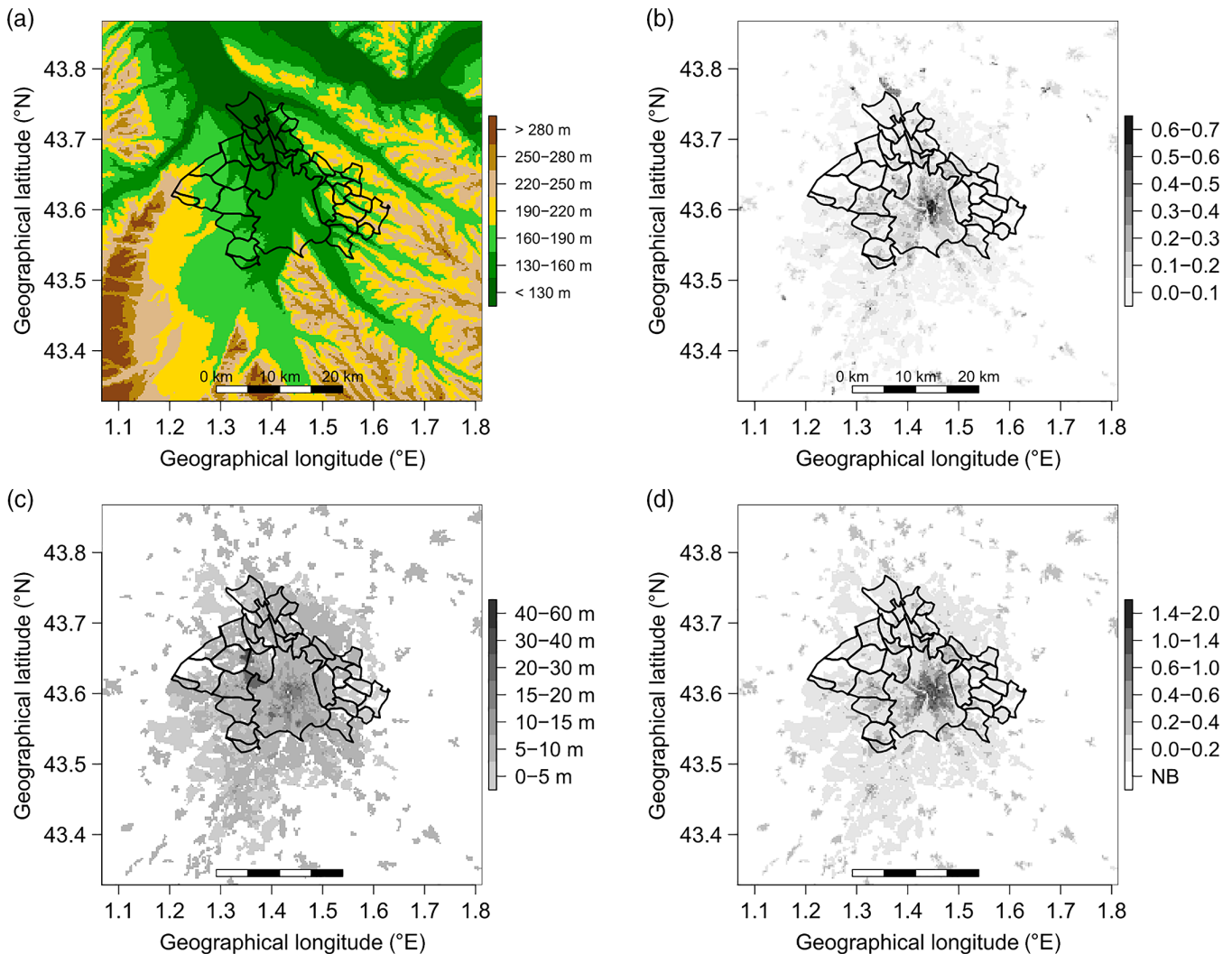


FIGURE 4 Spatial distribution in domain D4 of the (a) elevation above sea level, (b) building surface fraction, (c) average building height, and (d) façade surface density. Black lines indicate the boundaries of communes in the Toulouse Metropolitan Region [Colour figure can be viewed at wileyonlinelibrary.com]

the ground, over all the tiles is taken for the thermal climatic analysis. Due to the use of a big-leaf approach to model the urban vegetation, the specifics of the vertical profile of the near surface air temperature in tree canopies (LCZ A and B) cannot be represented. For MRT and UTCI, which are both related to human thermal comfort, they are not calculated on water bodies (SEA and WATER tiles) because the model assumes that inhabitants will not be located there. Therefore, results are not available for LCZ G (water) in the analyses involving MRT and UTCI. An approach to carefully select UTCI values from the TOWN or NATURE tiles is adopted when evaluating the potential heat stress experienced by people in different LCZs (Data S3 and Figure S1). Assuming that people are more likely to dwell in a built-up urban environment than in a rural environment, the TOWN tile UTCI is taken for model grids with a TOWN fraction of greater than or equal to 0.02; the NATURE tile UTCI is used otherwise.

3.2 | Evaluation of model results

The model results are evaluated with observations conducted during the CAPITOUL campaign (March 2004 to February 2005; Masson *et al.*, 2008). During this campaign, a mini-station network consisting of 21 stations was deployed in various districts that are representative of the urban environment. The stations were mounted on electrical towers at the border of the roads and the air temperature and relative humidity were measured (with a *HygroLog—1.0 rotronic hygroclip* sensor) every 12 min at 6 m above the ground. The observations made by the mini-station network should be comparable to the model results for the urban environment (TEB SBL levels). A second station network, known as the “synoptic network” here, measured the wind speed and direction at 10 m above the ground (*Young 05013* anemometer) as well as the up- and downwelling solar and terrestrial radiation at 2 m above the ground (*Schenk CM3* pyranometer) at locations outside the urban environment, which aim to be representative for the rather large scale meteorological conditions. They are used to evaluate the model results outside the urban environment.

The modelled air temperature and specific humidity in the urban environment are evaluated with the data from the mini-station network. The parameters modelled for the SBL level closest to 6 m (approximately 5 m) are compared with the observed values. Figure 5 shows the average values of T2M for the three time periods and the sensitivities of the observed and modelled temperatures with respect to the building surface fraction and the façade surface density. For all three time periods, the air temperature is higher in the centre of Toulouse compared to the suburban or rural areas (Figure 5, left column). The absolute value of the air

temperature is underestimated by approximately 2 K in both the urban and rural areas for EAFT and LAFT. At the same time, the specific humidity is overestimated by 1.5–2 g/kg during EAFT and LAFT, and by 1 g/kg during the NIGHT period (not shown). A potential reason for this deficiency is the initialization of soil moisture using the values from the ECMWF analysis. Differences in the soil texture or the soil model between MésoNH-SURFEX and the IFS model might lead to excessively high values for the soil moisture in MésoNH-SURFEX. The sensitivity of the air temperature with respect to the building surface fraction and façade surface density is captured well, especially for the NIGHT period when it is the largest. The observed specific humidity decreases slightly with the increasing building surface fraction and façade surface density. For EAFT and LAFT, MésoNH-TEB overestimates the dependency of the specific humidity on the degree of urbanization (not shown), which might be due to too much evapotranspiration in the rural areas.

The MRT cannot be evaluated directly because data are not available for the study period. However, it is possible to evaluate the diurnal cycle of the total (direct and diffusive) downwelling solar radiation and downwelling longwave radiation in open settings using a subset of stations from the synoptic station network that observed these variables and is located within D4 (Mondouzil, Toulouse-Météo, and Le Fauga; Figure 6a,b). The results show that the total downwelling shortwave radiation is underestimated by approximately 100 W/m² during the morning and at noon. During the same period, the downwelling longwave radiation is overestimated by 20–30 W/m². This result can be explained by an excessively large modelled cloud fraction. The modification of solar radiation by the buildings calculated by TEB has been evaluated by Redon *et al.* (2017) using the building resolving model SOLENE as a reference. Their results show that TEB accurately simulates the radiation captured by the wall and the ground. It is thus assumed that the radiation modification due to the buildings is captured well by TEB for the simplified urban geometry that is assumed. However, due to the street canyon geometry assumption, TEB cannot simulate the radiation heterogeneity due to the variety of building configurations at the district scale. In the real city, there are open places with a high SVF, but there are also very narrow streets with a very low SVF. TEB averages all these morphologies at the grid point scale, and as a result, it cannot represent the strong spatial variability of MRT at the sub-grid scale.

The modelled average diurnal cycle of the wind speed at 10 m above the ground (Figure 6c) is evaluated in a similar manner as the radiation components for the available stations from the synoptic station network (routine observation station at airport Toulouse Blagnac, Mondouzil, Toulouse-

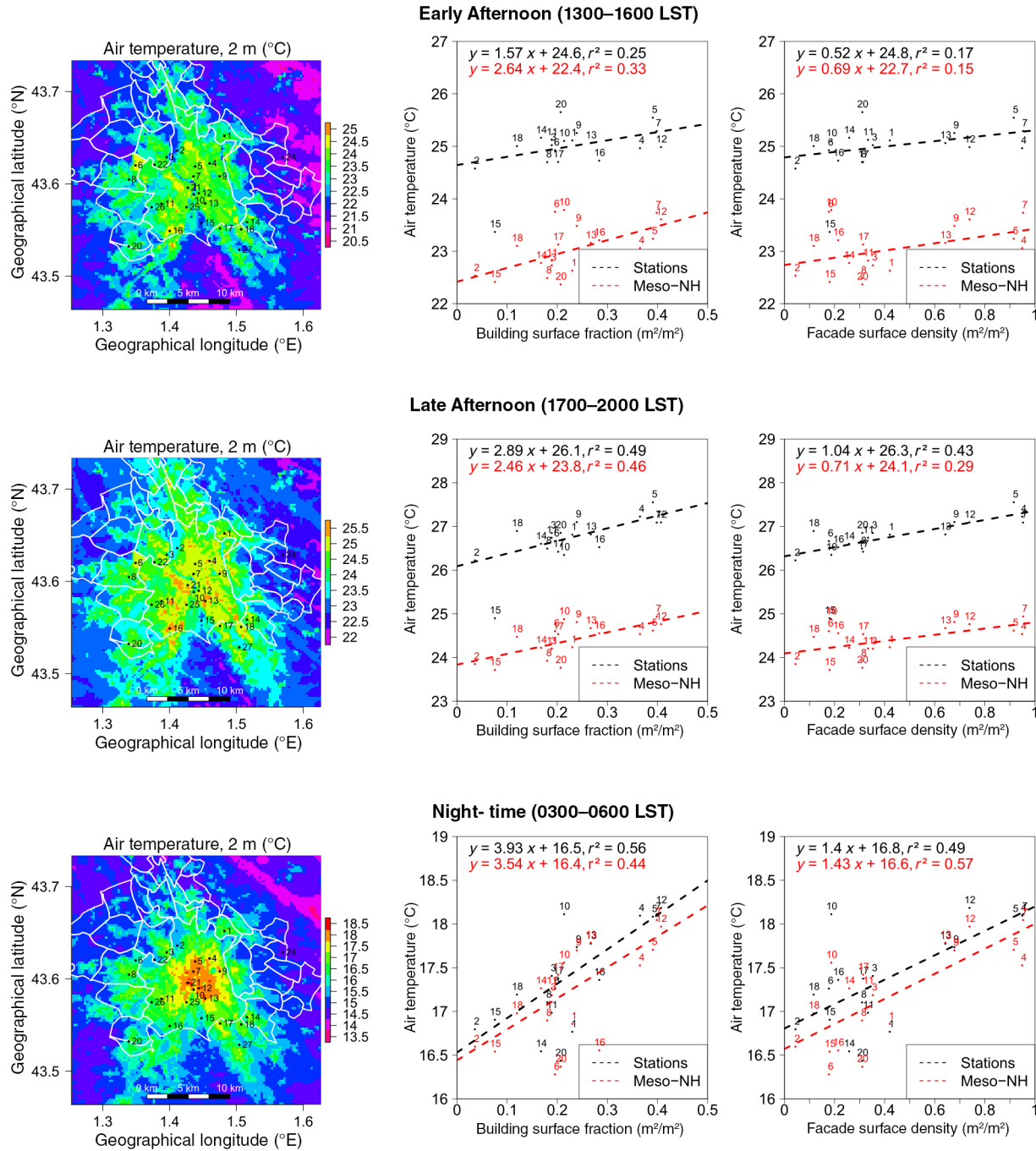


FIGURE 5 (left) Spatial distribution of modelled T2M in the Toulouse Metropolitan Region. The dots represent the location of the stations employed during the CAPITOU campaign. White lines indicate the boundaries of communes in the Toulouse Metropolitan Region. (middle and right) Modelled and observed air temperatures at the location of the stations plotted against building surface fraction and façade surface density. The temperature in the middle and right column is at 6 m above the ground and therefore the values do not correspond to those displayed in the left column [Colour figure can be viewed at wileyonlinelibrary.com]

Météo, and Auzerville). The prognostic value for the wind speed simulated at the first model level of Meso-NH at 10 m above the ground is used. The average wind speed is modelled accurately during the evening and night, but it is underestimated by up to 1 m/s (of 4 m/s) during the day. No observations are available for the wind speed in the street

canyon. The wind speed modelled by TEB represents the average in the urban canopy layer by accounting for the drag due to buildings. The vertical profile of the mixing length in the street canyon has been derived by Santiago and Martilli (2010) using building-resolving Reynolds-averaged Navier–Stokes simulations as a reference. It is thus assumed that the

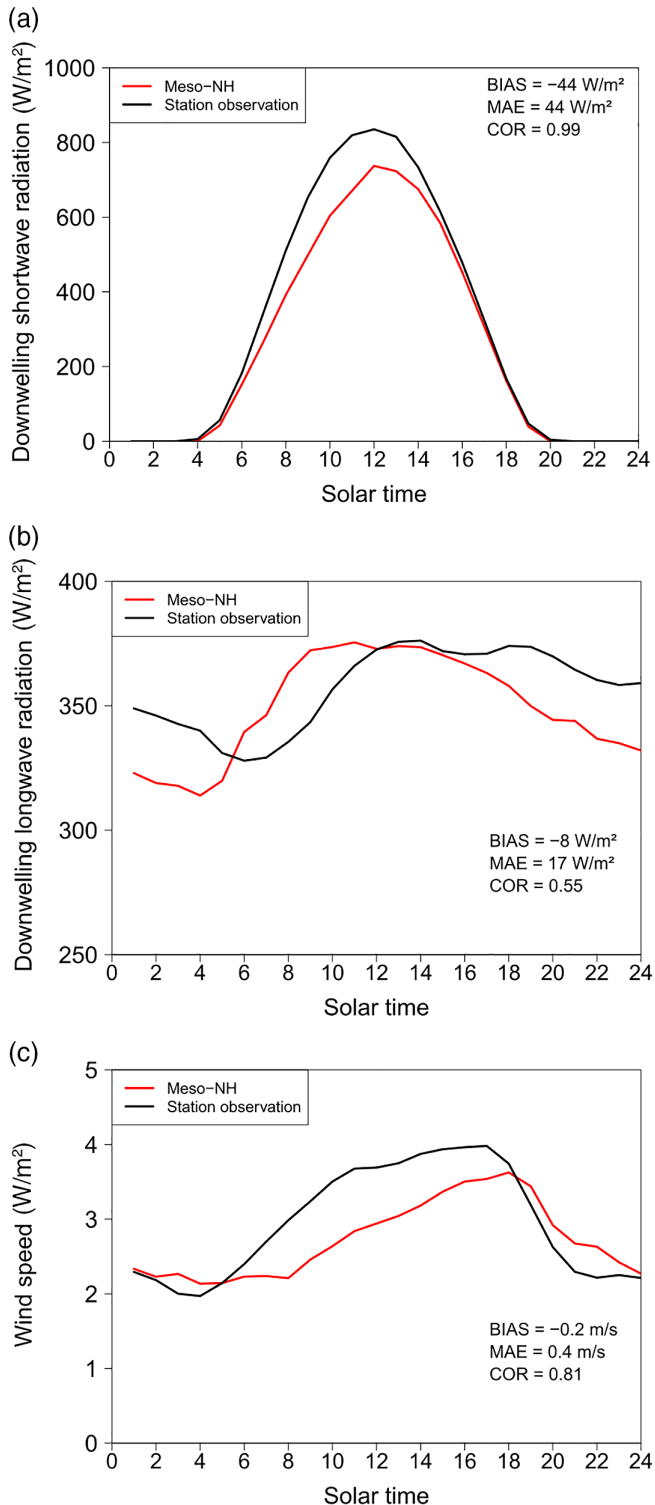


FIGURE 6 Evaluation of the modelled diurnal cycle averaged for all 18 days with weather type 9 (sunny and warm conditions, slight northwesterly wind) during summer 2004 of the (a) downwelling shortwave and (b) longwave radiation: observations are taken from the stations Mondouzil, Le Fauga and Météopole, and (c) wind speed: observations are taken from the stations Blagnac airport, Mondouzil, Météopole, and Auzeville. BIAS denotes the mean error (model output minus observed value), MAE the mean absolute error, and COR the Pearson correlation coefficient for modelled and observed diurnal cycle [Colour figure can be viewed at wileyonlinelibrary.com]

average modification of the wind speed due to the presence of buildings is modelled well, but its high spatial heterogeneity in the urban environment (e.g., due to channelling effects) cannot be captured by the modelling approach in use.

The primary implications for the urban thermal climatic analysis is that on the one hand, the air temperature is underestimated for the EAFT and LAFT, and so is the downwelling shortwave radiation for EAFT. These biases will tend to lead to an underestimation of the UTCI for these time periods. On the other hand, the wind speed is underestimated for the EAFT, which will tend to compensate for part of the underestimation in the UTCI due to the air temperature and downwelling shortwave radiation being too low. The sensitivity of the air temperature with respect to the urban morphology parameters is modelled well, which is encouraging for the analysis of the differences in meteorological parameters between LCZs.

4 | RESULTS AND DISCUSSION

4.1 | Thermal characteristics of LCZs in Toulouse

The thermal environment for different LCZs in the Toulouse Metropolitan Region is described by the T2M and MRT obtained from the Meso-NH simulations. In noting that there is a cold bias of approximately 2 K in the model, the discussions will focus more on the relative differences between LCZs rather than the absolute values of the thermal climatic parameters.

The statistical distributions of the T2M for the different LCZs at the three selected time periods are displayed in Figure 7a–c. A similar distribution across LCZs is observed for EAFT and LAFT, except that T2M is approximately 1 K higher during the LAFT for all the LCZs. At NIGHT, both the inter and intra-LCZ T2M ranges increase, which is consistent with previous findings on more prominent UHIs and larger intra-LCZ variabilities in cities at night (Alexander and Mills, 2014; Stewart *et al.*, 2014; Leconte *et al.*, 2015; Fenner *et al.*, 2017; Skarbit *et al.*, 2017). Generally, the T2M is higher for LCZ 1/2/3, LCZ 4/5, LCZ 6, and LCZ 8 (hereafter “built LCZs”) than for LCZ A, LCZ B, LCZ D, and LCZ G (hereafter “natural LCZs”). The only exception is the relatively high T2M in LCZ G (water) at NIGHT due to the high heat capacity of water. LCZ 9 (sparsely built) behaves more similarly to “natural LCZs” than to “built LCZs.” Among the “built LCZs,” LCZ 1/2/3 (compact settings) has the highest median T2M for all the time periods, followed by LCZ 4/5 (open high/mid-rise). LCZ 8 (large low-rise) has the highest maximum T2M and the third-highest median T2M during the day, but its temperature

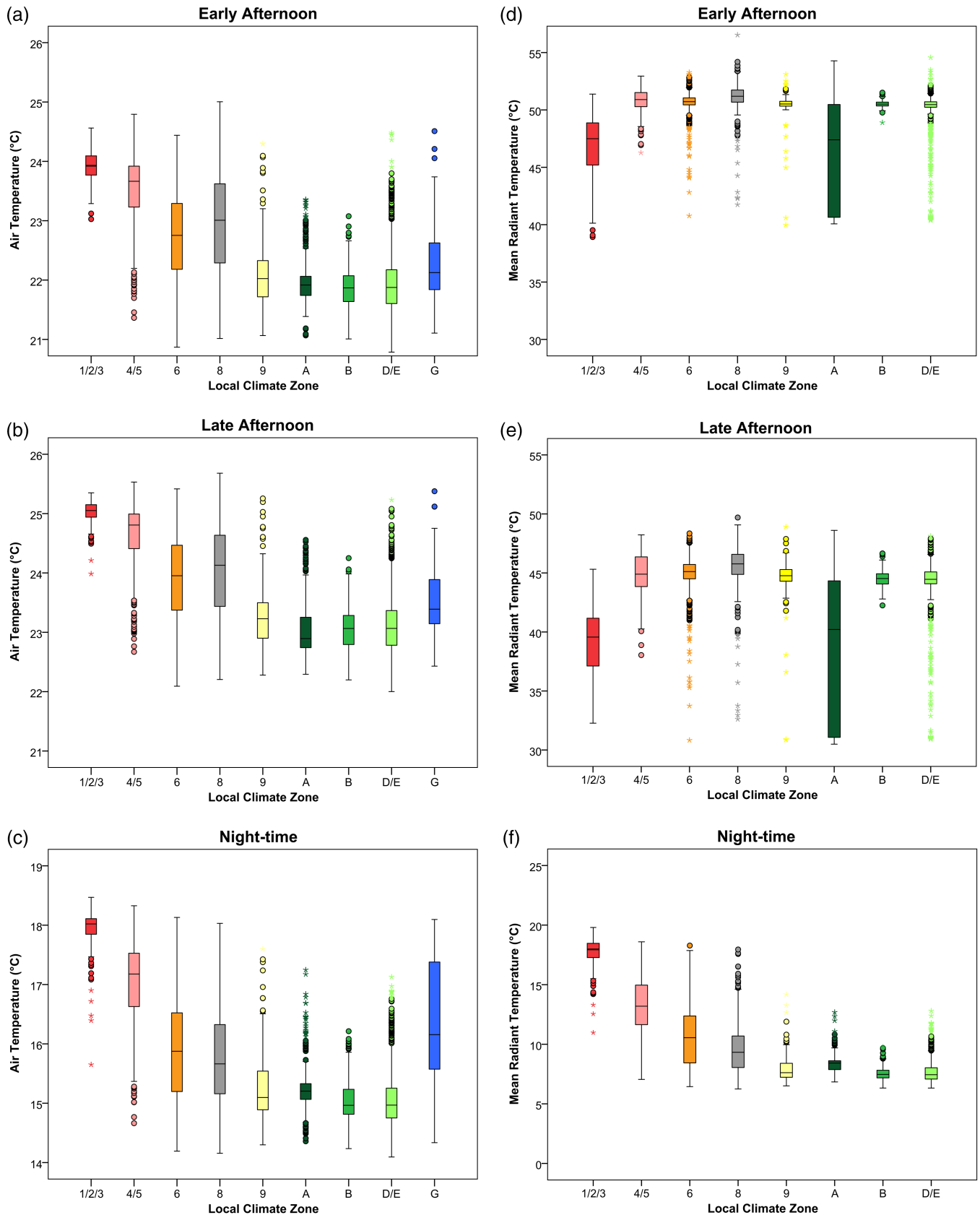


FIGURE 7 Distributions of modelled air temperature at 2 m above the ground and mean radiant temperature for different LCZs during the three selected time periods in the Toulouse Metropolitan Region. Note that subplots for different time periods have the same temperature range but different maximum/minimum values on the y-axis. Boxes show the median, and the first and third quartiles; whiskers show the highest/lowest value within 1.5 times the interquartile range; circles are outliers that fall above or below 1.5 times the interquartile range; asterisks are extreme outliers that fall above or below 3 times the interquartile range. Refer to Figure 2 for the number of data points for each LCZ group [Colour figure can be viewed at wileyonlinelibrary.com]

drops lower than that of LCZ 6 (open low-rise) at NIGHT probably due to its more open character (e.g., parking lots and bare ground). Large intra-LCZ variabilities are found for LCZ 6 and LCZ 8, which may be due to the heterogeneity in urban form owing to their locations at urban–rural boundaries, or simply as a result of the large number of data points (Figure 2). Interestingly, the large intra-LCZ variability for LCZ 6 is also observed in Berlin (Germany; Fenner *et al.*, 2017) and Szeged (Hungary; Skarbit *et al.*, 2017).

Figure 7d–f shows the MRT distributions for different LCZs. Overall, the MRT is the highest for EAFT when it is around solar noon. For EAFT and LAFT, median MRTs of all LCZs, except LCZ 1/2/3 and LCZ A, lie within a narrow range of 1.5 K. The compact urban structures and dense tree canopy provide shading and significantly lower the MRT for LCZ 1/2/3 and LCZ A. The median MRT is up to 6 K lower for LCZ 1/2/3 in the LAFT, when narrow street canyons are effectively shaded by buildings due to the low solar elevation angle. Although the median and maximum MRTs are similar for most LCZs, low outliers are observed, in particular for LCZs with more open settings (i.e., LCZ 6, LCZ 8, LCZ 9, and LCZ D/E). A further analysis reveals that they represent data points in the second Crown, which will be discussed in section 4.3. The statistical distribution of MRT across LCZs at NIGHT differs strongly from that during the day. The MRT for “built LCZs” is higher due to the emission of longwave radiation by the relatively warm construction materials and low SVF, especially in compact settings. The median MRT of LCZ 1/2/3 is up to 10.5 K higher than that of the other LCZs, and the MRT of “built LCZs” generally decreases according to the following order: LCZ 1/2/3, LCZ 4/5, LCZ 6, and LCZ 8. The statistical distribution of MRT for LCZ 9 is, again, more similar to “natural LCZs” than to “built LCZs.” The district-scale MRT obtained from the mesoscale model simulations employing the simplified street canyon geometry captures well the most relevant features; the lower MRT during the day in compact urban settings due to shading and the higher MRT during the night, due to the trapping of terrestrial infrared radiation. Nevertheless, an assessment of the MRT at a much higher resolution (e.g., 1 m) would be required to capture all the details of the MRT in the complex urban environment.

4.2 | Temperature differences among LCZs in Toulouse

The results of the Welch's ANOVA show that there is a statistically significant difference between the group means at the $\alpha = .05$ level overall. This finding indicates that the means of the T2M and MRT distributions are significantly different across LCZs, which can be explained by the differences in land cover and urban morphology. The

adjusted p -values from the Games-Howell post hoc test, along with the temperature differences in the mean T2M and MRT ($\Delta T2M_{\text{mean}}$ and ΔMRT_{mean}), are shown in Table 3a–f.

To allow for a simple interpretation of the results, pairs of LCZs that possess statistically significant different means in distributions of thermal climatic parameters based on the overall significance level of .05 after the Holm adjustment are considered to have “positive” results; otherwise, the results are considered “negative” (bold numbers in Table 3). “Positive” results of 89 and 82% are achieved overall for T2M and MRT, respectively. Pairs of LCZs with “positive” results generally correspond to a mean T2M difference larger than 10.2 K. In terms of the MRT, “positive” results may be explained by a large difference in either the mean MRT (up to a few K) or the variance for MRT distributions. In particular, “built LCZs” achieve 100% “positive” results for T2M, confirming the distinct T2M distributions modelled for these LCZs. It can thus be concluded that thermal characteristics, especially T2M, are indeed different across most LCZs, notably those relevant for urban areas, and that evaluating temperatures from numerical simulations using the LCZ scheme is an effective way to characterize the urban thermal environment of the Toulouse Metropolitan Region.

The means of T2M for all “built LCZs” are significantly different from other LCZs at any time of the day (Table 3a–c), although the $\Delta T2M_{\text{mean}}$ for LCZ 1/2/3 and LCZ 4 as well as LCZ 6 and LCZ 8 are rather small in magnitude. LCZ 9 has more similar T2M characteristics relative to “natural LCZs,” except for LCZ G, for which the T2M is higher at NIGHT. This finding alludes to the low impact on the local climate by small isolated clusters of buildings, given that they are surrounded by sufficient natural land covers. Vegetated covers in the Toulouse Metropolitan Region possess similar T2M distributions as suggested by the insignificant differences among LCZ A, LCZ B, and LCZ D/E, especially during the day. It should be noted, however, that these similarities might be overestimated due to the limitations of the LCZ mapping method (section 2.2) and model uncertainties (section 3.2) in the rural areas.

For the MRT (Table 3d–f), LCZ 1/2/3 and LCZ A behave similarly to one another, but they are both distinctly different from all the other LCZs during the day because of their ability to provide shading. The mean MRT of LCZ 1/2/3 and LCZ A can be up to 6.3 and 7.2 K lower than that of other LCZs in the LAFT. By contrast, the MRT distribution for LCZ 8 is also unique because of its lack of shading. However, compared to using the T2M, the LCZ scheme is less able to differentiate among zones according to their MRT signatures since LCZs with relatively open settings (i.e., LCZ 4/5, LCZ 6, LCZ 9, LCZ B, and LCZ D) display certain extent of similarity. At NIGHT, the means of the MRTs for all the “built LCZs” differ significantly from one

TABLE 3 Results of the Games-Howell post hoc test and the differences in mean values for air temperature at 2 m above ground ($\Delta T_{2M_{mean,x-y}}$) and mean radiant temperature ($\Delta MRT_{mean,x-y}$)

(a) Air temperature – early afternoon										
		<i>p</i> -Values from Games-Howell post hoc test								
LCZ (x)	LCZ (y)	1/2/3	4/5	6	8	9	A	B	D/E	G
$\Delta T_{2M_{mean,x-y}}$ (K)	1/2/3		.000	.000	.000	.000	.000	.000	.000	.000
	4/5	0.34		.000	.000	.000	.000	.000	.000	.000
	6	1.14	0.80		.000	.000	.000	.000	.000	.000
	8/10	0.90	0.55	-0.24		.000	.000	.000	.000	.000
	9	1.77	1.42	0.63	0.87		.199	.001	.090	.539
	A	1.90	1.56	0.77	1.01	0.14		.040	1.000	.001
	B	2.00	1.66	0.86	1.10	0.23	0.09		.026	.000
	D/E	1.92	1.57	0.78	1.02	0.15	0.01	-0.08		.000
	G	1.60	1.26	0.46	0.70	-0.17	-0.31	-0.40	-0.32	
(b) Air temperature – late afternoon										
		<i>p</i> -Values from Games-Howell post hoc test								
LCZ (x)	LCZ (y)	1/2/3	4/5	6	8	9	A	B	D/E	G
$\Delta T_{2M_{mean,x-y}}$ (K)	1/2/3		.000	.000	.000	.000	.000	.000	.000	.000
	4/5	0.35		.000	.000	.000	.000	.000	.000	.000
	6	1.07	0.72		.000	.000	.000	.000	.000	.000
	8/10	0.94	0.59	-0.13		.000	.000	.000	.000	.000
	9	1.71	1.35	0.63	0.77		.000	.001	.035	.020
	A	1.95	1.60	0.88	1.01	0.25		.979	.041	.000
	B	1.92	1.56	0.84	0.98	0.21	-0.04		.366	.000
	D/E	1.86	1.51	0.79	0.92	0.16	-0.09	-0.06		.000
	G	1.46	1.10	0.38	0.52	-0.25	-0.49	-0.46	-0.40	
(c) Air temperature – night-time										
		<i>p</i> -Values from Games-Howell post hoc test								
LCZ (x)	LCZ (y)	1/2/3	4/5	6	8	9	A	B	D/E	G
$\Delta T_{2M_{mean,x-y}}$ (K)	1/2/3		.000	.000	.000	.000	.000	.000	.000	.000
	4/5	0.82		.000	.000	.000	.000	.000	.000	.000
	6	1.95	1.13		.000	.000	.000	.000	.000	.008
	8/10	2.11	1.29	0.16		.000	.000	.000	.000	.000
	9	2.57	1.75	0.62	0.46		1.000	.000	.000	.000
	A	2.58	1.75	0.63	0.47	0.01		.000	.000	.000
	B	2.82	2.00	0.87	0.71	0.25	0.25		1.000	.000
	D/E	2.82	1.99	0.86	0.70	0.25	0.24	0.01		.000
	G	1.55	0.73	-0.40	-0.56	-1.02	-1.03	-1.27	-1.27	
(d) Mean radiant temperature – early afternoon										
		<i>p</i> -Values from Games-Howell post hoc test								
LCZ (x)	LCZ (y)	1/2/3	4/5	6	8	9	A	B	D/E	G
$\Delta MRT_{mean,x-y}$ (K)	1/2/3		.000	.000	.000	.000	.000	.355	.000	.000

TABLE 3 (Continued)

(d) Mean radiant temperature – early afternoon									
		<i>p</i> -Values from Games-Howell post hoc test							
LCZ (x)	LCZ (y)	1/2/3	4/5	6	8	9	A	B	D/E
	4/5	−3.93		.714	.000	.045	.000	.000	.000
	6	−3.83	0.09		.000	.141	.000	.000	.000
	8/10	−4.32	−0.40	−0.49		.000	.000	.000	.000
	9	−3.45	0.48	0.39	0.88		.000	.912	1.000
	A	0.80	4.72	4.63	5.12	4.24		.000	.000
	B	−3.63	0.30	0.20	0.69	−0.18	−4.43		.000
	D	−3.37	0.55	0.46	0.95	0.07	−4.17	0.26	
(e) Mean radiant temperature – late afternoon									
		<i>p</i> -Values from Games-Howell post hoc test							
LCZ (x)	LCZ (y)	1/2/3	4/5	6	8	9	A	B	D/E
$\Delta MRT_{\text{mean},x-y}$ (K)	1/2/3		.000	.000	.000	.000	.514	.000	.000
	4/5	−5.47		.540	.000	.613	.000	.017	.000
	6	−5.66	−0.19		.000	.077	.000	.000	.000
	8/10	−6.29	−0.82	−0.64		.000	.000	.000	.000
	9	−5.07	0.40	0.58	1.22		.000	1.000	.964
	A	0.89	6.36	6.54	7.18	5.96		.000	.000
	B	−5.12	0.35	0.54	1.17	−0.05	−6.00		.005
	D	−4.85	0.62	0.80	1.44	0.22	−5.74	0.27	
(f) Mean radiant temperature – night-time									
		<i>p</i> -Values from Games-Howell post hoc test							
LCZ (x)	LCZ (y)	1/2/3	4/5	6	8	9	A	B	D/E
$\Delta MRT_{\text{mean},x-y}$ (K)	1/2/3		.000	.000	.000	.000	.000	.000	.000
	4/5	4.20		.000	.000	.000	.000	.000	.000
	6	6.84	2.64		.000	.000	.000	.000	.000
	8/10	7.91	3.72	1.07		.000	.000	.000	.000
	9	9.39	5.20	2.56	1.48		.263	.003	.015
	A	9.10	4.90	2.26	1.18	−0.30		.000	.000
	B	9.87	5.67	3.03	1.95	0.47	0.77		.834
	D	9.81	5.61	2.97	1.89	0.41	0.71	−0.06	

Notes: Bold numbers highlight *p*-values and corresponding temperature differences of LCZ pairs which are not significantly different from each other after the Holm adjustments.

another, while the mean of the MRT for LCZ 9 is similar to that of LCZ A.

The nocturnal air temperature difference between LCZ *X* (where *X* = 1 to 10) and LCZ D (ΔT_{X-D}) is often used to quantify the UHI intensity in cities (Alexander and Mills, 2014; Stewart *et al.*, 2014; Leconte *et al.*, 2015; Fenner *et al.*, 2017; Skarbit *et al.*, 2017). The mean $\Delta T_{2M_{X-D}}$ at NIGHT obtained in this study range from 0.25 K for

$\Delta T_{2M_{9-D}}$ to 2.82 K for $\Delta T_{2M_{1/2/3-D}}$ (Table 3c). These values fall on the lower end when compared with those reported in observational studies conducted in other European cities (see summary table of Skarbit *et al.*, 2017). This may be attributable to the fact that the modelled values are being averaged over time (18 days*4 hr for each time period) and space (all data points of the same LCZ in the three regions), rather than taken from specific point

measurements at contrasting locations on a few ideal days. However, an evaluation of the modelled results against observations during the CAPITOU campaign in Houet and Pigeon's (2011) study indicates the good resemblance of the difference in thermal characteristics across LCZs and the corresponding UCZs with similar land cover and urban morphology, especially for the differences in the daily minimum air temperature in the summer (Data S4 and Table S1,S2). Thus, the modelled results are considered to reflect the UHI present under typical summer conditions in the Toulouse Metropolitan Region.

4.3 | Regional changes among inter- and intra-LCZ thermal differences

This section presents a further analysis on the inter- and intra-LCZ variabilities of thermal climatic parameters within the Toulouse Metropolitan Region by separately analysing the T2M and MRT distributions of LCZs in the Toulouse Municipality, first Crown, and second Crown. The results are shown as box plots in Figure 8 for T2M and Figure 9 for MRT. Since the prevalence of LCZs differ for the three regions, some LCZs need to be further grouped based on similarities in their urban forms (e.g., LCZs 2, 3, 4, and 5 for the first Crown) and natural features (e.g., LCZs A and B for the Toulouse Municipality) to avoid sample sizes that are too small (Table 4).

In reference to Figure 8, it is clear that although the T2M differs between the LCZs within each region, there are intra-LCZ T2M differences for the different regions. There is a general decrease in the T2M for all the LCZs with the increasing distance from the city centre, reflecting a systematic change in urban morphological indicators for the same LCZ as observed by Hidalgo *et al.* (2019). They found that indicators such as the building height, building surface fraction, impervious surface fraction, and aspect ratio for the same LCZ are generally lower in the periphery than in the city centre. These changes are well-captured by the shift in T2M distributions, resulting in intra-LCZ variations of approximately 2 K for “built LCZs” during EAFT and LAFT, and even more at NIGHT. It is also interesting to note that LCZs bear rather different distributions in the T2M when located at different parts of the city. For example, in terms of T2M, LCZ 9 in the Toulouse Municipality has a similar signature to LCZ 6 in the first Crown, while LCZ 9 in the first Crown behaves similarly as LCZ 6 in the second Crown. In addition to the different values of the urban morphological indicators, the advection of warm air from the neighbouring LCZ 1/2/3 to less built-up LCZs may be another contributing factor to the intra-LCZ T2M variations (Quanz *et al.*, 2018). Since Toulouse is located in a valley, the difference in elevation between the three regions could

also be responsible for the decrease of the T2M with increasing distance to the city centre. However, the average terrain height differs by less than 20 m between Toulouse Municipality and the second Crown and can therefore not explain the intra-LCZ T2M difference of almost 1.5 K.

The intra-LCZ differences among the three regions for “natural LCZs” are less pronounced (approximately 1 K). There are few trees (grouped as LCZ A/B) in the Toulouse Municipality, but they can exhibit a T2M that is more than 2 K lower than LCZ 1/2/3 is at NIGHT, providing local cool zones for heat stress relief in the city centre. For the second Crown, though it is cooler overall, the T2M difference between LCZ 3/5 and vegetated “natural LCZs” (LCZ A, LCZ B, and LCZ D) is only approximately 0.5 K. However, not all “natural LCZs” are able to moderate the night-time air temperature. For areas with water bodies (LCZ G), the T2M may be higher than it is for most “built LCZs” (LCZ 4/5, LCZ 6, LCZ 8) at NIGHT, particularly in the Toulouse Municipality (Figure 8c). This finding is consistent with previous studies on the adverse effect of urban water bodies on UHI and thermal comfort during warm summer nights (Theeuwes *et al.*, 2013; Steeneveld *et al.*, 2014).

MRT (Figure 9) is less influenced by advection than T2M, and it does not vary much during EAFT and LAFT as a function of the distance to the city centre. Nevertheless, certain features characteristic of each region can still be observed. The shading effect by compact urban structures (LCZ 1/2/3) is only found in Toulouse Municipality, where dense buildings and narrow street canyons are common in the historic city centre. The urban morphology (Figure 2) and surface relief (Figure 1a) of the first Crown are comparatively homogeneous and flat, comprising primarily open low-rise (LCZ 6) residential areas, large low-rise (LCZ 8) warehouses and low plants (LCZ D). This configuration gives rise to the narrow MRT ranges and relatively uniform MRT distributions across LCZs, especially for EAFT (Figure 9d). In the second Crown, the MRT of LCZ A is significantly lower, probably due to the concentration of trees in the Bouconne Forest. There are also many low outliers for LCZ 6, LCZ 8, and LCZ D in the second Crown. Because the terrain is more hilly in the second Crown, particularly in the east (Figure 1a), the solar radiation reaching the land surface may be less even, causing more shading in the valleys and thus in areas with a lower MRT. At NIGHT, a higher MRT is observed in the Toulouse Municipality, especially for LCZ 1/2/3, due to the larger amount of stored heat released from the buildings (Figure 9c). This leads to a greater MRT difference between “built LCZs” and “natural LCZs” in Toulouse Municipality compared to in the first and second Crowns.

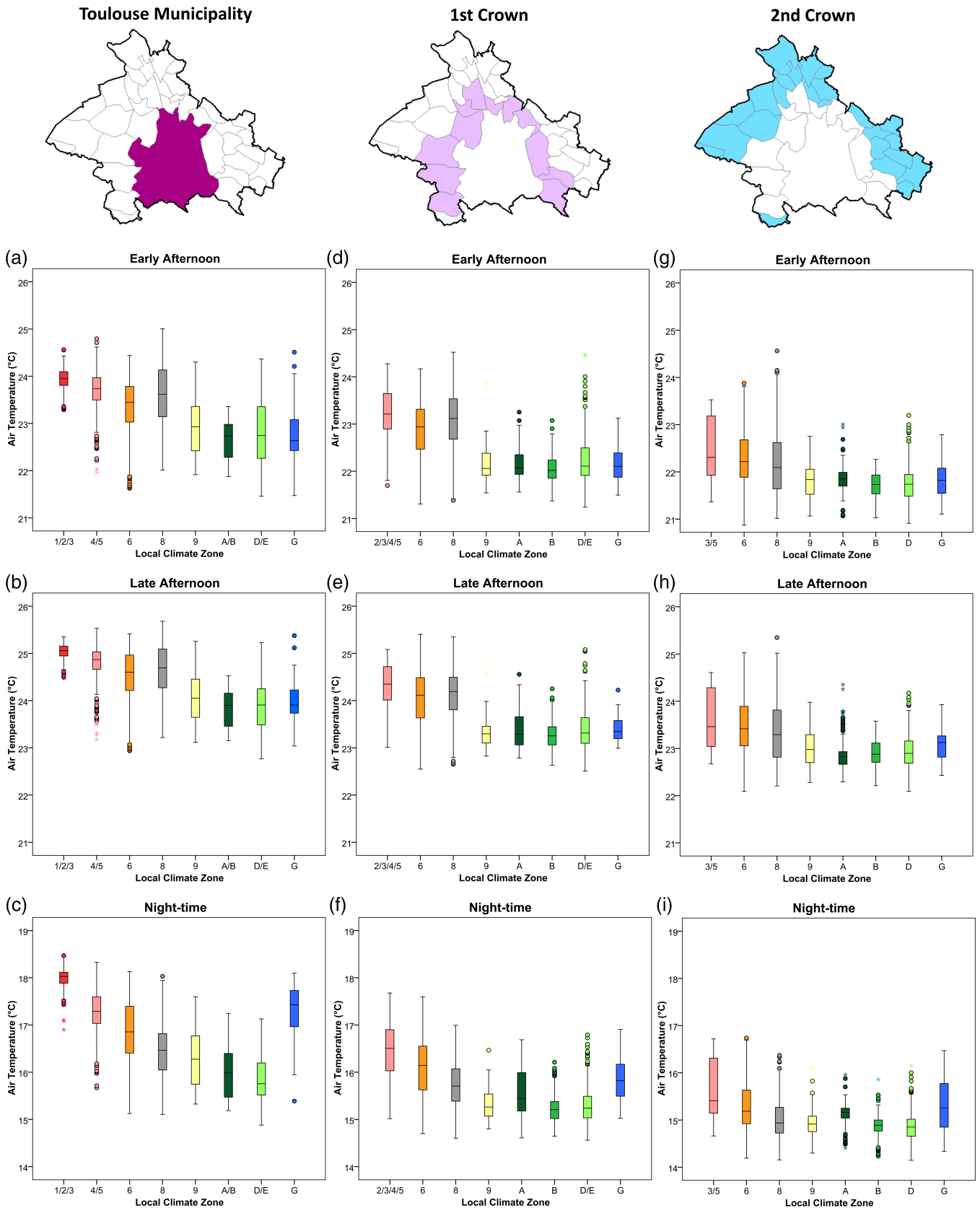


FIGURE 8 Distributions of modelled air temperature at 2 m above the ground for different LCZs in (a–c) the Toulouse Municipality, (d–f) first Crown, and (g–i) second Crown during the three selected time periods. Note that the LCZ groups on the *x*-axis are not exactly the same as in Figure 7 and for the three zones due to the uneven prevalence of LCZs. Also note that subplots for different time periods have the same temperature range but different maximum/minimum values on the *y*-axis. Refer to Table 4 for the number of data points for each LCZ group. Refer to Figure 7 caption for a description of the elements in the boxplots [Colour figure can be viewed at wileyonlinelibrary.com]

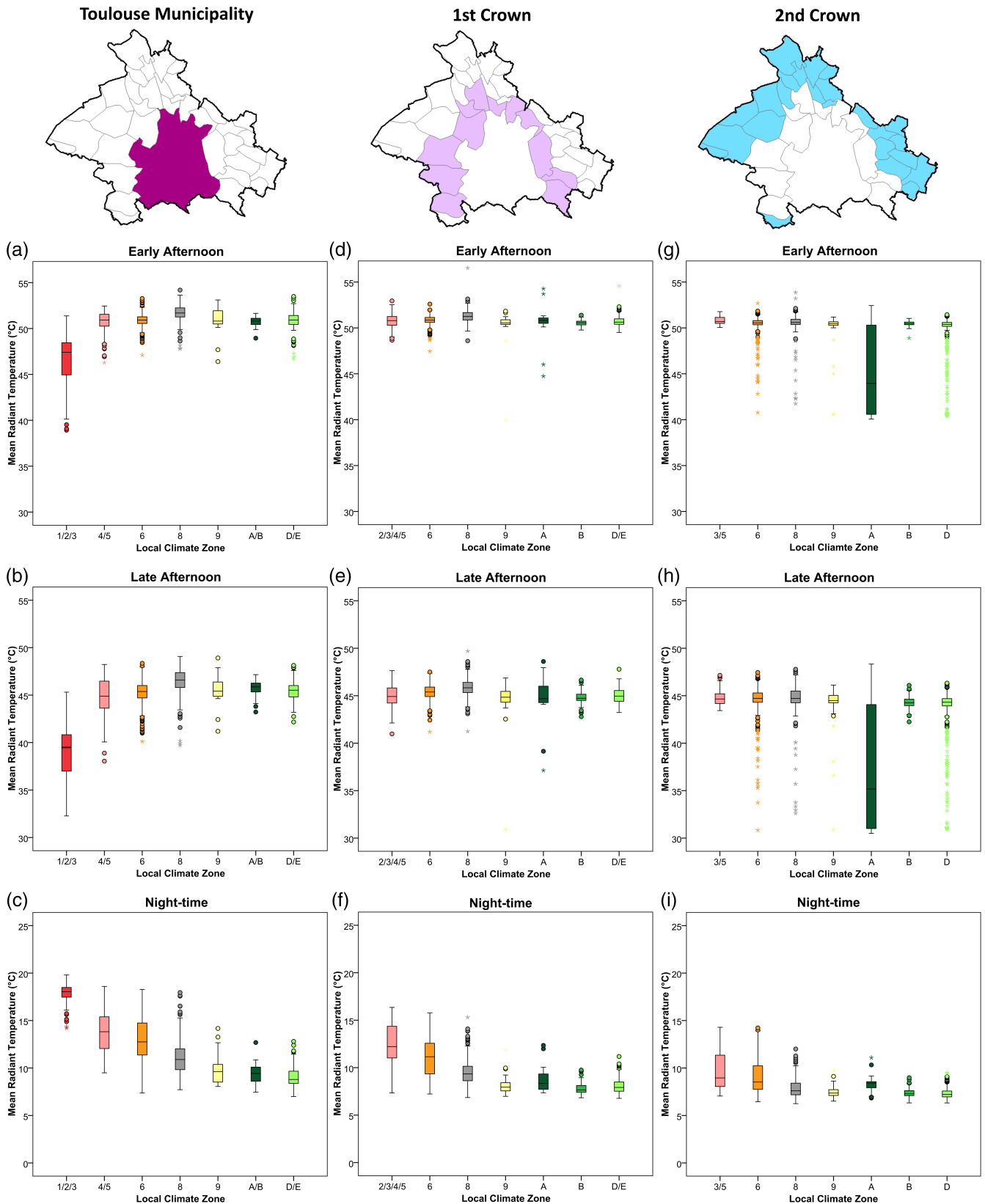


FIGURE 9 Distributions of modelled mean radiant temperature for different LCZs in (a–c) the Toulouse Municipality, (d–f) first Crown, and (g–i) second Crown during the three selected time periods. Note that the LCZ groups on the x-axis are not exactly the same as in Figure 7 and for the three zones due to the uneven prevalence of LCZs. Also note that subplots for different time periods have the same temperature range but different maximum/minimum values on the y-axis. Refer to Table 4 for the number of data points for each LCZ group. Refer to Figure 7 caption for a description of the elements in the boxplots [Colour figure can be viewed at wileyonlinelibrary.com]

TABLE 4 The number and frequency of data points for each LCZ group in (a) Toulouse Municipality, (b) first Crown, and (c) second Crown

(a) Toulouse Municipality (1,878 data points)								
LCZ (grouped)	1/2/3	4/5	6	8	9	A/B	D/E	G
No. of data points	165	319	592	540	26	32	159	45
% in region	8.8	17.0	31.5	28.8	1.4	1.7	8.5	2.4
(b) First Crown (2,203 data points)								
LCZ (grouped)	2/3/4/5	6	8	9	A	B	D/E	G
No. of data points	62	1,044	478	44	62	118	366	29
% in region	2.8	47.4	21.7	2.0	2.8	5.4	16.6	1.3
(c) Second Crown (3,250 data points)								
LCZ (grouped)	3/5	6	8	9	A	B	D	G
No. of data points	24	1,157	497	90	251	165	1,037	29
% in region	0.7	35.6	15.3	2.8	7.7	5.1	31.9	0.9

4.4 | Thermal stress and LCZs

The thermal stress that people may experience in different LCZs is evaluated according to the UTCI assessment scale (Table 1). The frequency and severity of thermal stress for different LCZs are presented as stacked bars in Figure 10. Under typical summer conditions, people in the outdoor environment of the Toulouse Metropolitan Region experience substantial amounts of heat stress, for all the LCZs. In the EAFT, the probability of strong/very strong heat stress for all “built LCZs” is above 20%: it is the highest for LCZ 4/5 (23.3%), followed by LCZ 8 (22.9%) and LCZ 6 (22%). The probability of moderate heat stress is also the highest for LCZ 4/5 (58.2%), followed by LCZ 1/2/3 (55.8%). During this time period, people may find heat stress relief in LCZ A, where the probability of no thermal stress is almost 50%. In the LAFT, the probability of heat stress is generally lower for all the LCZs. The stress remains the highest for LCZ 4/5 but the probabilities of strong/very heat stress and moderate heat stress are lowered to 17.7 and 47%, respectively. Meanwhile, the probability of strong/very strong heat stress for LCZ 1/2/3 drops to the lowest among the “built LCZs” (12.8%) due to the shading effects of the buildings. Regarding “natural LCZs,” their thermal conditions are significantly improved during LAFT, particularly for LCZ A which now has a probability of more than 60% of having no thermal stress.

For the NIGHT period, there is almost no outdoor heat stress for all the LCZs. There is even a 10–20% probability of slight cold stress for “natural LCZs” and LCZ 9. However, the problem at night, especially for dense urban areas, occurs when the residual heat from the day is trapped indoors, causing sustained high indoor air temperatures that could affect the quality of sleep and the recovery of the human body

from the daytime heat gain (Laaidi *et al.*, 2012; Ji *et al.*, 2014). Therefore, assessing night-time thermal comfort with the UTCI may be insufficient for reflecting the heat risks faced by residents.

Previous studies that evaluated the outdoor human thermal comfort for different LCZs mostly employed the PET index, which is generally comparable to the UTCI for hot European climate conditions (Matzarakis *et al.*, 2014). Their findings are in good agreement with the results of the current study. For an inner-city neighbourhood in Oberhausen (Germany), Müller *et al.* (2014) found particularly high PET values for LCZ 5 and LCZ 2 and low PET values for LCZ A due to a combination of shading and evapotranspiration. Similarly, Unger *et al.* (2018) found the highest PET for LCZ 5, LCZ 2, and LCZ 3 based on long-term observations in Szeged (Hungary). Milošević *et al.* (2016) studied the thermal comfort conditions for different LCZs during a heatwave period in Novi Sad (Serbia). They reported high thermal loads for LCZ 5, LCZ D, and LCZ 3 and lower thermal loads for LCZ A and LCZ 2 in the morning. They also noted a delayed peak in PET values for LCZ 2 due to the shading effects of the buildings. Using HUMIDEX to quantify outdoor human thermal comfort, Geletič *et al.* (2018) concluded that the most thermally uncomfortable areas within Brno (Czech Republic) were all built LCZs, apart from LCZ 4 and LCZ 9, which probably benefited from shading associated with high-rise buildings and a high proportion of vegetated areas. With reference to all the above studies, one may conclude that LCZ 5 is the area that is most prone to heat stress, while LCZ A and LCZ 9 are thermally more pleasant zones. Buildings in compact urban settings (LCZ 1/2/3) can lower the MRT by providing shading, and thus they provide a certain extent of heat stress relief during the daytime.

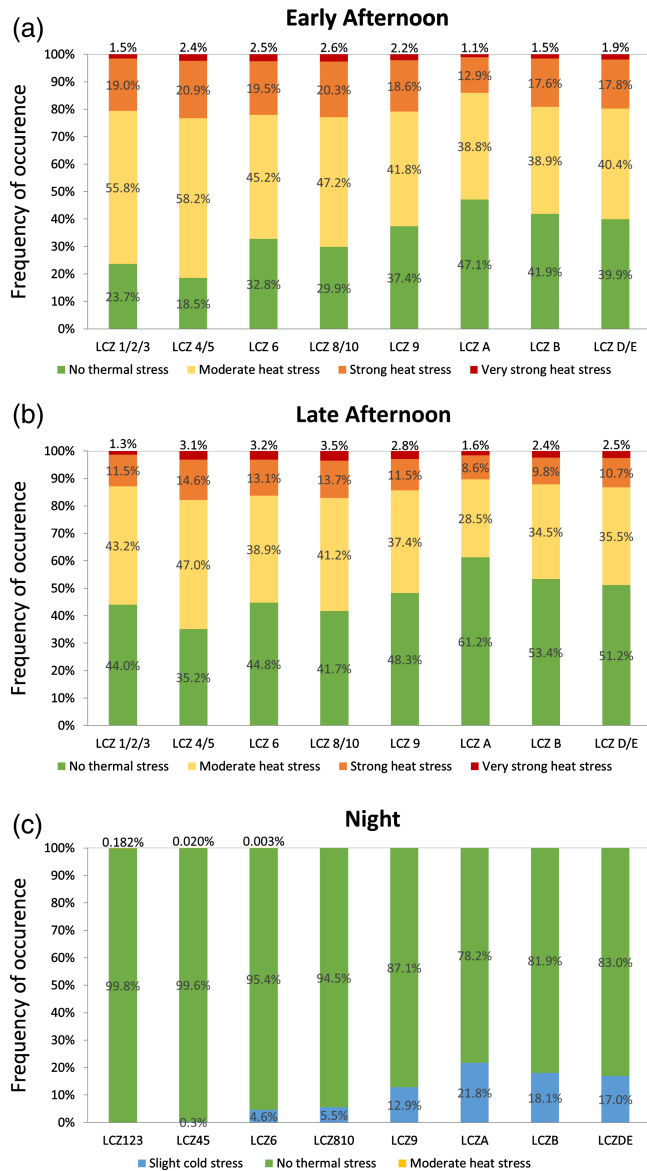


FIGURE 10 Frequencies and severities of thermal stress, inferred from modelled UTCI, for different LCZs during the three selected time periods in the Toulouse Metropolitan Region [Colour figure can be viewed at wileyonlinelibrary.com]

5 | CONCLUSION

This study investigates the spatiotemporal variation of three thermal climatic parameters, namely the air temperature at 2 m above the ground (T2M), the mean radiant temperature (MRT), and the Universal Thermal Climate Index (UTCI), as modelled with the mesoscale atmospheric model Méso-NH for typical summer conditions in the Toulouse Metropolitan Region. There is also an examination of whether the local climate zone (LCZ) classification is suited to distinguishing among the distributions of the modelled parameters. This approach is valid because the LCZ map has not been used to define the model input parameters related to

urban morphology, and the sensitivity of the modelled air temperature with respect to urban morphological parameters has been captured accurately.

The LCZ scheme is generally able to discern the thermal environment of the Toulouse Metropolitan Region in terms of the T2M. The T2M distributions are distinct between LCZs, notably for “built LCZs” (LCZ 1/2/3, LCZ 4/5, LCZ 6 and LCZ 8). Consistent with the observations and previous studies, the highest T2M is found for compact urban settings (LCZ 1/2/3), and the mean nocturnal UHI intensity can be up to 2.8 K. However, the intra-LCZ T2M variability can be quite high for LCZ 6 (open low-rise) and LCZ 8 (large low-rise), suggesting that the LCZ scheme might be lacking in details needed for characterizing the urban–rural interface of Toulouse. Furthermore, the T2M decreases as a function of the distance from the city centre, owing to a systematic change in urban morphological indicators, even for the same LCZ.

The LCZ scheme is less able to differentiate among zones according to their MRT distributions because the inter-LCZ difference in the MRT is relatively small for LCZs with open settings during the day. The only exceptions are for LCZ 1/2/3 and LCZ A (dense trees), both of which exhibit a lowered MRT due to shading effects. At night, the MRT distribution reflects the differential emission of stored heat and the trapping of terrestrial infrared radiation, and it is the highest for LCZ 1/2/3. Finally, the thermal stress that people may experience in different LCZs is evaluated according to the UTCI assessment scale. The probability of heat stress is the highest for LCZ 4/5 (open high/mid-rise) during the day, while the probability of heat stress is consistently the lowest for LCZ A. LCZ 9 (sparsely built) is also more favourable from the perspective of heat stress mitigation.

This study provided a holistic understanding of local variability in the thermal climate within the urban environment of Toulouse. It also demonstrated the advantages of using numerical simulation data for conducting urban climatic analyses, including its city-wide spatial coverage and the availability of thermal climatic parameters other than the air temperature. Nevertheless, while the analysis for warm and dry summer conditions (WT9) may be sufficient for evaluating days when the area is most susceptible to heat stress, considering the plurality of weather situations would be required for a holistic understanding of the seasonally varying urban thermal environment. Assumptions and uncertainties in the model simulations, such as the underestimation of meteorological parameters relevant for heat stress, have also been reported. Besides, shading by street trees in the urban area has not been considered, limiting the evaluation of the effectiveness of the existing heat stress mitigation features within the city.

Moving forwards, this urban climatic analysis approach could be applied to other cities in France, or it could even be extended to cities with LCZs mapped around the world, thanks to the World Urban Database and Access Portal Tools initiative (Ching *et al.*, 2018). Further work should also explore how urban climatic analysis results could be incorporated into larger urban planning frameworks alongside other considerations, such as demographics, urban development, energy use, public health, economic activities, and transport infrastructure.

ACKNOWLEDGEMENTS

This work is supported by The Vice-Chancellor's Discretionary Fund of The Chinese University of Hong Kong. It has also received support from the French National Agency of Research for the project applied Modelling and urban Planning laws: Urban Climate and Energy (MApUCE) under reference ANR-13-VBDU-0004.

ORCID

Yu Ting Kwok  <https://orcid.org/0000-0002-3612-748X>

REFERENCES

- Alexander, P.J. and Mills, G. (2014) Local climate classification and Dublin's urban heat Island. *Atmosphere*, 5(4), 755–774.
- Aminipouri, M., Knudby, A.J., Krayenhoff, E.S., Zickfeld, K. and Middel, A. (2019) Modelling the impact of increased street tree cover on mean radiant temperature across Vancouver's local climate zones. *Urban Forestry & Urban Greening*, 39, 9–17.
- Arnfield, A.J. (2003) Two decades of urban climate research: a review of turbulence, exchanges of energy and water, and the urban heat Island. *International Journal of Climatology*, 23(1), 1–26.
- ASHRAE. (2013) *Fundamentals Handbook*. Atlanta: ASHRAE.
- Bechtel, B., Alexander, P.J., Böhner, J., Ching, J., Conrad, O., Feddema, J., Mills, G., See, L. and Stewart, I. (2015) Mapping local climate zones for a worldwide database of the form and function of cities. *ISPRS International Journal of Geo-Information*, 4(1), 199–219.
- Beck, C., Straub, A., Breitner, S., Cyrus, J., Philipp, A., Rathmann, J., Schneider, A., Wolf, K. and Jacobeit, J. (2018) Air temperature characteristics of local climate zones in the Augsburg urban area (Bavaria, southern Germany) under varying synoptic conditions. *Urban Climate*, 25, 152–166.
- Blanca, M., Alarcón, R., Arnau, J., Bono, R. and Bendayan, R. (2017) Non-normal data: Is ANOVA still a valid option? *Psicothema*, 29(4), 552–557.
- Blazejczyk, K., Jendritzky, G., Bröde, P., Fiala, D., Havenith, G., Epstein, Y., Psikuta, A. and Kampmann, B. (2013) An introduction to the universal thermal climate index (UTCI). *Geographia Polonica*, 86(1), 5–10.
- Bocher, E., Petit, G., Bernard, J. and Palominos, S. (2018) A geoprocessing framework to compute urban indicators: the MApUCE tools chain. *Urban Climate*, 24, 153–174.
- Bougeault, P. and Lacarrere, P. (1989) Parameterization of orography-induced turbulence in a mesobeta-scale model. *Monthly Weather Review*, 117(8), 1872–1890.
- Buechley, R.W., Van Bruggen, J. and Truppi, L.E. (1972) Heat island = death island? *Environmental Research*, 5(1), 85–92.
- Bueno, B., Pigeon, G., Norford, L.K., Zibouche, K. and Marchadier, C. (2012) Development and evaluation of a building energy model integrated in the TEB scheme. *Geoscientific Model Development*, 5, 433–448.
- Champeaux, J., Masson, V. and Chauvin, F. (2005) ECOCLIMAP: a global database of land surface parameters at 1 km resolution. *Meteorological Applications*, 12(1), 29–32.
- Ching, J., Mills, G., Bechtel, B., See, L., Feddema, J., Wang, X., Ren, C., Brousse, O., Martilli, A., Neophytou, M., Mouzoudires, P., Stewart, I., Hanna, A., Ng, E., Foley, M., Alexander, P., Aliaga, D., Niyogi, D., Shreevastava, A., Bhalachandran, S., Masson, V., Hidalgo, J., Fung, J., de Fatima Andrad, M., Baklanov, A., Wei Dai, D., Milcinski, G., Demuzere, M., Brunzell, N., Pesaresi, M., Miao, S., Mu, Q., Chen, F. and Theeuwes, N. (2018) *World Urban Database and Access Portal Tools (WUDAPT): an urban weather, climate and environmental modeling infrastructure for the anthropocene*. Boston: Bulletin of the American Meteorological Society.
- Cleugh, H. and Grimmond, S. (2012) Urban climates and global climate change. In: Henderson-Sellers, A. and McGuffie, K. (Eds.) *The Future of the World's Climate*. Oxford, UK: Elsevier, pp. 47–76.
- Conti, S., Meli, P., Minelli, G., Solimini, R., Toccaceli, V., Vichi, M., Beltrano, C. and Perini, L. (2005) Epidemiologic study of mortality during the summer 2003 heat wave in Italy. *Environmental Research*, 98(3), 390–399.
- Crombette, P., Le Corre, S. and Tinel, C. (2014) Traitement d'images satellitaires à très haute résolution spatiale et identification de zones à enjeux dans l'aménagement des trames vertes urbaines. *Revue Française De Photogrammétrie Et De Télédétection*, 208, 19–25.
- Deardorff, J.W. (1980) Stratocumulus-capped mixed layers derived from a three-dimensional model. *Boundary-Layer Meteorology*, 18(4), 495–527.
- Erell, E. and Williamson, T. (2007) Intra-urban differences in canopy layer air temperature at a mid-latitude city. *International Journal of Climatology*, 27(9), 1243–1255.
- European Centre for Medium-Range Weather Forecasts (ECMWF). (2019) *Changes in ECMWF model—evolution of the IFS, 2019*. Reading, UK: ECMWF. Available at: <https://www.ecmwf.int/en/forecasts/documentation-and-support/changes-ecmwf-model>.
- Fenner, D., Meier, F., Bechtel, B., Otto, M. and Scherer, D. (2017) Intra and inter local climate zone variability of air temperature as observed by crowdsourced citizen weather stations in Berlin, Germany. *Meteorologische Zeitschrift*, 26, 525–547.
- Fouillet, A., Rey, G., Laurent, F., Pavillon, G., Bellec, S., Guihenneuc-Jouyaux, C., Clavel, J., Jouglu, E. and Hémon, D. (2006) Excess mortality related to the August 2003 heat wave in France. *International Archives of Occupational and Environmental Health*, 80(1), 16–24.
- Gabriel, K.M. and Endlicher, W.R. (2011) Urban and rural mortality rates during heat waves in Berlin and Brandenburg, Germany. *Environmental Pollution*, 159(8–9), 2044–2050.

- Games, P.A. and Howell, J.F. (1976) Pairwise multiple comparison procedures with unequal n's and/or variances: a Monte Carlo study. *Journal of Educational Statistics*, 1(2), 113–125.
- Geletič, J. and Lehnert, M. (2016) GIS-based delineation of local climate zones: the case of medium-sized central European cities. *Moravian Geographical Reports*, 24(3), 2–12.
- Geletič, J., Lehnert, M., Savić, S. and Milošević, D. (2018) Modelled spatiotemporal variability of outdoor thermal comfort in local climate zones of the city of Brno, Czech Republic. *Science of the Total Environment*, 624, 385–395.
- Gosling, S.N., Lowe, J.A., McGregor, G.R., Pelling, M. and Malamud, B.D. (2009) Associations between elevated atmospheric temperature and human mortality: a critical review of the literature. *Climatic Change*, 92(3–4), 299–341.
- Grimmond, C.S.B., Blackett, M., Best, M.J., Barlow, J., Baik, J., Belcher, S.E., Bohnenstengel, S.I., Calmet, I., Chen, F., Dandou, A., Fortuniak, K., Gouvea, M.L., Hamdi, R., Hendry, M., Kawai, T., Kawamoto, Y., Kondo, H., Krayenhoff, E.S., Lee, S., Loridan, T., Martilli, A., Masson, V., Miao, S., Oleson, K., Pigeon, G., Porson, A., Ryu, Y., Salamanca, F., Shashua-Bar, L., Steeneveld, G., Tombrou, M., Voogt, J., Young, D. and Zhang, N. (2010) The international urban energy balance models comparison project: first results from phase 1. *Journal of Applied Meteorology and Climatology*, 49(6), 1268–1292.
- Grize, L., Huss, A., Thommen, O., Schindler, C. and Braun-Fahrlander, C. (2005) Heat wave 2003 and mortality in Switzerland. *Swiss Medical Weekly*, 135(13–14), 200–205.
- Hamdi, R. and Masson, V. (2008) Inclusion of a drag approach in the town energy balance (TEB) scheme: offline 1D evaluation in a street canyon. *Journal of Applied Meteorology and Climatology*, 47(10), 2627–2644.
- Hidalgo, J., Dumas, G., Masson, V., Petit, G., Bechtel, B., Bocher, E., Foley, M., Schoetter, R. and Mills, G. (2019) Comparison between local climate zones maps derived from administrative datasets and satellite observations. *Urban Climate*, 27, 64–89.
- Hidalgo, J. and Jouglu, R. (2018) On the use of local weather types classification to improve climate understanding: an application on the urban climate of Toulouse. *PLoS One*, 13(12), e0208138.
- Hidalgo, J., Masson, V. and Baehr, C. (2014) From daily climatic scenarios to hourly atmospheric forcing fields to force soil–vegetation–atmosphere transfer models. *Frontiers in Environmental Science*, 2, 40.
- Hidalgo, J., Pigeon, G. and Masson, V. (2008) Urban-breeze circulation during the CAPITOU experiment: observational data analysis approach. *Meteorology and Atmospheric Physics*, 102(3–4), 223–241.
- Holm, S. (1979) A simple sequentially rejective multiple test procedure. *Scandinavian Journal of Statistics*, 6, 65–70.
- Houet, T. and Pigeon, G. (2011) Mapping urban climate zones and quantifying climate behaviors—an application on Toulouse urban area (France). *Environmental Pollution*, 159(8), 2180–2192.
- Institut national de la statistique et des études économiques (Insee). (2016) *Définition—urban unit, 2019*. Insee, France: National Institute of Statistics and Economic Studies. Available at: <https://www.insee.fr/en/metadonnees/definition/c1501>.
- Ji, Y., Fitton, R., Swan, W. and Webster, P. (2014) Assessing overheating of the UK existing dwellings—a case study of replica Victorian end terrace house. *Building and Environment*, 77, 1–11.
- Kain, J.S. and Fritsch, J.M. (1990) A one-dimensional entraining/detraining plume model and its application in convective parameterization. *Journal of Atmospheric Sciences*, 47(23), 2784–2802.
- Kleerekoper, L., Van Esch, M. and Salcedo, T.B. (2012) How to make a city climate-proof, addressing the urban heat island effect. *Resources, Conservation and Recycling*, 64, 30–38.
- Koppe, C., Sari Kovats, R., Menne, B., Jendritzky, G., Wetterdienst, D. and World Health Organization. (2004) *Heat-waves: risks and responses (No. 2)*. Copenhagen: WHO Regional Office for Europe.
- Kovács, A. and Németh, Á. (2012) Tendencies and differences in human thermal comfort in distinct urban areas in Budapest, Hungary. *Acta Climatologica et Chorologica*, 46, 115–124.
- Laaidi, K., Zeghnoun, A., Dousset, B., Bretin, P., Vandentorren, S., Giraudet, E. and Beaudou, P. (2012) The impact of heat islands on mortality in Paris during the August 2003 heat wave. *Environmental Health Perspectives*, 120(2), 254–259.
- Lac, C., Chaboureau, J., Masson, V., Pinty, J., Tulet, P., Escobar, J., Leriche, M., Barthe, C., Aouizerats, B., Augros, Cl., Aumond, P., Auguste, F., Bechtold, P., Berthet, S., Bielli, S., Bosseurs, F., Caumont, O., Cohard, J., Colin, J., Couvreur, F., Cuxart, J., Delautier, G., Dauhut, T., Ducrocq, V., Filippi, J., Gazen, D., Geoffroy, O., Gheusi, F., Honnert, R., Lafore, J., Brossier, C., Libois, Q., Lunet, T., Mari, C., Maric, T., Mascart, P., Mogé, M., Molinié, G., Nuissier, O., Pantillon, F., Peyrillé, P., Pergaud, J., Perraud, E., Pianezze, J., Redelsperger, J., Ricard, D., Richard, E., Riette, S., Rodier, Q., Schoetter, R., Seyfried, L., Stein, J., Suhre, K., Taufour, M., Thouron, O., Turner, S., Verrelle, A., Vié, B., Visentin, F., Vionnet, Vi. and Wautelet, P. (2018) Overview of the meso-NH model version 5.4 and its applications. *Geoscientific Model Development Discussions*, 11, 1929–1969. <https://doi.org/10.5194/gmd-11-1929-2018>.
- Leconte, F., Bouyer, J., Claverie, R. and Pétrissans, M. (2015) Using local climate zone scheme for UHI assessment: evaluation of the method using mobile measurements. *Building and Environment*, 83, 39–49.
- Lehnert, M., Geletič, J., Husák, J. and Vysoudil, M. (2015) Urban field classification by “local climate zones” in a medium-sized central European city: the case of Olomouc (Czech Republic). *Theoretical and Applied Climatology*, 122(3–4), 531–541.
- Lelovics, E., Unger, J. and Gál, T. (2014) Design of an urban monitoring network based on local climate zone mapping and temperature pattern modelling. *Climate Research*, 60, 51–62.
- Lemonsu, A., Masson, V., Shashua-Bar, L., Erell, E. and Pearlmutter, D. (2012) Inclusion of vegetation in the town energy balance model for modelling urban green areas. *Geoscientific Model Development*, 5(6), 1377–1393.
- Lin, T. (2009) Thermal perception, adaptation and attendance in a public square in hot and humid regions. *Building and Environment*, 44(10), 2017–2026.
- Lix, L.M., Keselman, J.C. and Keselman, H.J. (1996) Consequences of assumption violations revisited: a quantitative review of alternatives to the one-way analysis of variance *F* test. *Review of Educational Research*, 66(4), 579–619.
- Masson, V. (2000) A physically-based scheme for the urban energy budget in atmospheric models. *Boundary-Layer Meteorology*, 94(3), 357–397.
- Masson, V., Gomes, L., Pigeon, G., Liousse, C., Pont, V., Lagouarde, J., Voogt, J., Salmond, J., Oke, T.R. and Hidalgo, J. (2008) The canopy and aerosol particles interactions in Toulouse

- Urban Layer (CAPITOU) experiment. *Meteorology and Atmospheric Physics*, 102(3–4), 135–157.
- Masson, V., Hidalgo, J., Amossé, A., Belaid, F., Bocher, E., Bonhomme, M., Bourgeois, A., Bretagne, G., Caillerez, S., Cordeau, E. and Demazeux, C. (2015) *Urban climate, human behavior & energy consumption: from LCZ mapping to simulation and urban planning (the MApUCE project), 20-24 July 2015*. Paper presented at the 9th International Conference on Urban Climate, Toulouse, France.
- Masson, V., Le Moigne, P., Martin, E., Faroux, S., Alias, A., Alkama, R., Belamari, S., Barbu, A., Boone, A., Bouyssel, F., Brousseau, P., Brun, E., Calvet, J.-C., Carrer, D., Decharme, B., Delire, C., Donier, S., Essauini, K., Gibelin, A.-L., Giordani, H., Habets, F., Jidane, M., Kerdraon, G., Kourzeneva, E., Lafaysse, M., Lafont, S., Lebeaupin Brossier, C., Lemonsu, A., Mahfouf, J.-F., Marguinaud, P., Mokhtari, M., Morin, S., Pigeon, G., Salgado, R., Seity, Y., Taillefer, F., Tanguy, G., Tulet, P., Vincendon, B., Vionnet, V. and Voldoire, A. (2013) The SURFEXv7.2 land and ocean surface platform for coupled or offline simulation of earth surface variables and fluxes. *Geoscientific Model Development*, 6, 929–960.
- Matzarakis, A., Muthers, S. and Rutz, F. (2014) Application and comparison of UTCI and PET in temperate climate conditions. *Finisterra: Revista Portuguesa de Geografia*, 49(98), 21–31.
- Middel, A., Häb, K., Brazel, A.J., Martin, C.A. and Guhathakurta, S. (2014) Impact of urban form and design on mid-afternoon microclimate in Phoenix local climate zones. *Landscape and Urban Planning*, 122, 16–28.
- Milošević, D.D., Savić, S.M., Marković, V., Arsenović, D. and Šćerov, I. (2016) Outdoor human thermal comfort in local climate zones of Novi Sad (Serbia) during heat wave period. *Hungarian Geographical Bulletin*, 65(2), 129–137.
- Müller, N., Kuttler, W. and Barlag, A.B. (2014) Counteracting urban climate change: adaptation measures and their effect on thermal comfort. *Theoretical and Applied Climatology*, 115(1–2), 243–257.
- Noilhan, J. and Planton, S. (1989) A simple parameterization of land surface processes for meteorological models. *Monthly Weather Review*, 117(3), 536–549.
- Oke, T.R. (1981) Canyon geometry and the nocturnal urban heat Island: comparison of scale model and field observations. *International Journal of Climatology*, 1(3), 237–254.
- Oke, T.R. (2004) *Initial guidance to obtain representative meteorological observations at urban sites*. Geneva: World Meteorological Organization, IOM Report 81, WMO/TD-No. 1250.
- Oke, T.R., Mills, G., Christen, A. and Voogt, J.A. (2017) *Urban Climates*. Cambridge: Cambridge University Press.
- Pergaud, J., Masson, V., Malardel, S. and Couvreur, F. (2009) A parameterization of dry thermals and shallow cumuli for mesoscale numerical weather prediction. *Boundary-Layer Meteorology*, 132(1), 83–106.
- Quanz, J.A., Ulrich, S., Fenner, D., Holtmann, A. and Eimermacher, J. (2018) Micro-scale variability of air temperature within a local climate zone in Berlin, Germany, during summer. *Climate*, 6(1), 5.
- Redon, E.C., Lemonsu, A., Masson, V., Morille, B. and Musy, M. (2017) Implementation of street trees within the solar radiative exchange parameterization of TEB in SURFEX v8.0. *Geoscientific Model Development*, 10(1), 385–411.
- Santiago, J. and Martilli, A. (2010) A dynamic urban canopy parameterization for mesoscale models based on computational fluid dynamics Reynolds-averaged Navier–Stokes microscale simulations. *Boundary-Layer Meteorology*, 137(3), 417–439.
- Schoetter, R., Masson, V., Bourgeois, A., Pellegrino, M. and Lévy, J. (2017) Parametrisation of the variety of human behaviour related to building energy consumption in the town energy balance (SURFEX-TEB v. 8.2). *Geoscientific Model Development*, 10(7), 2801–2831.
- Sharmin, T., Steemers, K. and Matzarakis, A. (2015) Analysis of microclimatic diversity and outdoor thermal comfort perceptions in the tropical megacity Dhaka, Bangladesh. *Building and Environment*, 94, 734–750.
- Skarbit, N., Stewart, I.D., Unger, J. and Gál, T. (2017) Employing an urban meteorological network to monitor air temperature conditions in the “local climate zones” of Szeged, Hungary. *International Journal of Climatology*, 37(S1), 582–596.
- Steenefeld, G., Koopmans, S., Heusinkveld, B. and Theeuwes, N. (2014) Refreshing the role of open water surfaces on mitigating the maximum urban heat island effect. *Landscape Urban Plann.* 121, 92–96. <https://doi.org/10.1016/j.landurbplan.2013.09.001>.
- Stewart, I.D. (2011) A systematic review and scientific critique of methodology in modern urban heat island literature. *International Journal of Climatology*, 31(2), 200–217.
- Stewart, I.D. and Oke, T.R. (2012) Local climate zones for urban temperature studies. *Bulletin of the American Meteorological Society*, 93(12), 1879–1900.
- Stewart, I.D., Oke, T.R. and Kravayehoff, E.S. (2014) Evaluation of the “local climate zone” scheme using temperature observations and model simulations. *International Journal of Climatology*, 34(4), 1062–1080.
- Tan, J., Zheng, Y., Tang, X., Guo, C., Li, L., Song, G., Zhen, X., Yuan, D., Kalkstein, A.J., Li, F. and Chen, H. (2010) The urban heat island and its impact on heat waves and human health in Shanghai. *International Journal of Biometeorology*, 54(1), 75–84.
- Theeuwes, N.E., Solcerová, A. and Steeneveld, G.J. (2013) Modeling the influence of open water surfaces on the summertime temperature and thermal comfort in the city. *J. Geophys. Res.-Atmos.* 118(16), 8881–8896. <https://doi.org/10.1002/jgrd.50704>.
- Tornay, N., Schoetter, R., Bonhomme, M., Faraut, S. and Masson, V. (2017) GENIUS: a methodology to define a detailed description of buildings for urban climate and building energy consumption simulations. *Urban Climate*, 20, 75–93.
- Unger, J., Skarbit, N. and Gál, T. (2018) Evaluation of outdoor human thermal sensation of local climate zones based on long-term database. *International Journal of Biometeorology*, 62(2), 183–193.
- Van Hove, L.W.A., Jacobs, C.M.J., Heusinkveld, B.G., Elbers, J.A., Van Driel, B.L. and Holtslag, A.A.M. (2015) Temporal and spatial variability of urban heat island and thermal comfort within the Rotterdam agglomeration. *Building and Environment*, 83, 91–103.
- Verdonck, M., Van Coillie, F., De Wulf, R., Okujeni, A., van der Linden, S., Demuzere, M. and Hooyberghs, H. (2017) *Thermal evaluation of the local climate zone scheme in Belgium, 6-8 March 2017*. Paper presented at the Urban Remote Sensing Event (JURSE), 2017 Joint, Dubai, United Arab Emirates.
- Verdonck, M.L., Demuzere, M., Hooyberghs, H., Beck, C., Cyrus, J., Schneider, A., Dewulf, R. and van Coillie, F. (2018) The potential of local climate zones maps as a heat stress assessment tool, supported by simulated air temperature data. *Landscape and Urban Planning*, 178, 183–197.

- Villadiego, K. and Velay-Dabat, M.A. (2014) Outdoor thermal comfort in a hot and humid climate of Colombia: a field study in Barranquilla. *Building and Environment*, 75, 142–152.
- Welch, B.L. (1951) On the comparison of several mean values: an alternative approach. *Biometrika*, 38(3/4), 330–336.

SUPPORTING INFORMATION

Additional supporting information may be found online in the Supporting Information section at the end of this article.

How to cite this article: Kwok YT, Schoetter R, Lau KK-L, *et al.* How well does the local climate zone scheme discern the thermal environment of Toulouse (France)? An analysis using numerical simulation data. *Int J Climatol*. 2019;39:5292–5315. <https://doi.org/10.1002/joc.6140>